

Gestational Stress Induces the Unfolded Protein Response Resulting in Heart Defects

Hongjun Shi^{1,5}, Victoria C. O'Reilly¹, Julie L.M. Moreau¹, Therese R. Bewes¹, Michelle X. Yam¹, Bogdan E. Chapman^{2,§}, Stuart M. Grieve^{2,3,4}, Roland Stocker^{1,6}, Robert M. Graham^{1,5,6}, Gavin Chapman^{1,5}, Duncan B. Sparrow^{1,5,7} and Sally L. Dunwoodie^{1,5,6,7}

1. The Victor Chang Cardiac Research Institute, Sydney, NSW, 2010, Australia

2. School of Molecular Bioscience, University of Sydney, Sydney, NSW, 2006, Australia

3. Sydney Translational Imaging Laboratory, Sydney Medical School, University of Sydney, Sydney, 2006, NSW, Australia

4. Department of Radiology, Royal Prince Alfred Hospital, Sydney, NSW, 2050, Australia

5. St Vincent's Clinical School, Faculty of Medicine, University of New South Wales, Sydney, NSW, 2010, Australia

6. School of Biotechnology and Biomolecular Sciences, Faculty of Science, University of New South Wales, Sydney, NSW, 2052, Australia

7. co-senior and co-corresponding author

Contacts: Sally Dunwoodie, 405 Liverpool Street, Darlinghurst, NSW, 2010, Australia. Tel: +612 9295 8613. Email: s.dunwoodie@victorchang.edu.au; Duncan Sparrow. Email: duncan.sparrow@dpag.ox.ac.uk

§ We remember B.E. Chapman and his important contribution to this research (1948-2014).

Running Title: Gestational stress and heart development

SUMMARY STATEMENT

Gestational hypoxia impairs heart development in mice and may be a cause of congenital heart disease in humans.

29 ABSTRACT

30 Congenital heart disease (CHD) is an enigma. It is the most common human birth defect, and yet, even
31 with the application of modern genetic and genomic technologies, only a minority of cases can be
32 explained genetically. This is because environmental stressors also cause CHD. Here we propose a
33 plausible non-genetic mechanism for induction of CHD by environmental stressors. We show that
34 exposure of mouse embryos to short-term gestational hypoxia induces the most common types of heart
35 defect. This is mediated by the rapid induction of the unfolded protein response (UPR), which profoundly
36 reduces FGF signaling in cardiac progenitor cells of the second heart field. Thus UPR activation during
37 human pregnancy may be a common cause of CHD. Our findings have far-reaching consequences
38 because the UPR is activated by a myriad of environmental or pathophysiological conditions. Ultimately,
39 our discovery could lead to preventative strategies to reduce the incidence of human CHD.

41 INTRODUCTION

42 Congenital heart disease (CHD) is an abnormality in the heart's structure or function that arises before
43 birth. It is the most common form of human birth defect, with an incidence of around 9 per 1,000 live
44 births (van der Linde et al., 2011). The etiology of CHD is complex, with both genetic and environmental
45 factors playing a role. Genetic factors have been widely investigated (reviewed in (Andersen et al., 2014);
46 (Fahed et al., 2013). However, only ~20% of CHD cases can be attributed to a specific genetic cause
47 (Blue et al., 2012). Thus non-genetic factors are likely to be important in human heart development. This
48 idea is supported by the large phenotypic variability seen between individuals with the same genetic
49 mutation (Schott et al., 1998; Benson et al., 1999), and this is also true with variable heart defects in
50 inbred mice (Abu-Issa et al., 2002). **Epidemiological studies have identified significant environmental**
51 **risk factors for human CHD, including maternal exposures to alcohol, isotretinoin, thalidomide,**
52 **antiseizure medications, antiretroviral medications, environmental teratogens and infectious agents.**
53 Embryo hypoxia is another well recognized risk factor caused by smoking, living at high altitude,
54 maternal diabetes, high body mass index, hypertension or prescription medications.(Watkins et al., 2003;
55 Jenkins et al., 2007; Zheng et al., 2013; Webster et al., 2014; Ornoy et al., 2015; Ramakrishnan et al.,
56 2015; Sullivan et al., 2015). The specific effects of environment on embryonic development have been
57 studied by exposing pregnant animals to a variety of conditions. Hypoxia has been studied in this way for
58 almost 200 years, causing a variety of birth defects, including heart defects (Geoffroy Saint Hilaire, 1820;
59 Ingalls et al., 1952; Sparrow et al., 2012). We have recently shown that short-term gestational hypoxia
60 significantly increases the penetrance and severity of vertebral defects in mouse models of congenital
61 scoliosis (Sparrow et al., 2012). At the molecular level, hypoxia disrupts embryonic FGF signaling,
62 leading to a temporary failure of somitogenesis.

63 Heart formation in vertebrates has been well studied (reviewed in (Miquerol and Kelly, 2013). The
64 linear heart tube forms from the first heart field (FHF). These cells contribute mainly to the left ventricle

65 and both atria of the mature heart. The linear heart tube elongates and loops to the right, driven by the
66 addition of second heart field (SHF) cells to the arterial and venous poles. These cells contribute mostly
67 to the right ventricle and inflow/outflow regions of the heart. The proliferation of SHF cells is controlled
68 by FGF and β -catenin/WNT signaling, and their subsequent differentiation is controlled by BMP and
69 non-canonical WNT pathways. Perturbation of proliferation, or premature activation of differentiation or
70 apoptosis, for example by conditional deletion of FGF signaling components in the SHF, results in OFT
71 elongation, alignment and septation defects (Hutson et al., 2006; Ilagan et al., 2006; Park et al., 2006). In
72 humans such defects include membranous ventricular septal defects (VSD); persistent truncus arteriosus
73 (PTA); double outlet right ventricle (DORV); transposition of the great arteries (TGA); overriding aorta
74 (OA) and Tetralogy of Fallot (TOF), and account for as much as 30-60% of all human CHD (Thom et al.,
75 2006; Bruneau, 2008).

76 Here we present evidence that short-term gestational hypoxia can perturb mammalian heart
77 formation, resulting in defects of OFT alignment and/or elongation. We show that hypoxic exposure
78 results in reduced cellular proliferation in the SHF and elsewhere. In the SHF this is likely to be due to a
79 downregulation of FGF signaling, mediated by the specific loss of the receptor FGFR1. We show that
80 hypoxia induces the unfolded protein response (UPR), causing a global downregulation of protein
81 translation. Since FGFR1 protein has a short half-life (Haugsten et al., 2005), this results in rapidly
82 reduced receptor and signaling levels. Our findings may provide a mechanism for the genesis of some of
83 the 80% of cases of human CHD that remain unexplained by a purely genetic etiology. This mechanism is
84 also likely to apply to birth defects in addition to CHD, as FGF signaling is required for numerous
85 processes during embryogenesis.

86

87 RESULTS

88 ***In utero* exposure of mouse embryos to lowered oxygen levels perturbs cardiac outflow tract** 89 **formation**

90 We investigated if exposure of mouse embryos to hypoxia *in utero* induces heart defects. Previous studies
91 exposing mice to hypoxia (Ingalls et al., 1952) induced a low rate of ventricular septal defects (VSDs).
92 We performed similar experiments using more extreme hypoxia to maximize the rate of induced heart
93 defects. Mice can tolerate as low as 5.5% oxygen at normal atmospheric pressure (Sparrow et al., 2012).
94 We therefore exposed pregnant C57BL/6J mice to 5.5% oxygen for 8 hours (hypoxia), and then returned
95 them to room air (normoxia) until embryonic day (E) 17.5 when embryonic heart morphology was
96 examined (Table 1). Groups of pregnant mice were exposed on different days encompassing heart
97 development (E7.5-10.5). Heart defects were observed in some embryos exposed from E8.5-E10.5, with a
98 statistically significant peak at E9.5 At this stage 21/48 embryos had heart defects. By contrast, low
99 oxygen exposure did not significantly increase the incidence of embryo death, except at E10.5. All
00 abnormal embryos exposed at E9.5 (21/21) had defects typical of a disruption of outflow tract (OFT)

01 alignment or elongation (VSD, OA, DORV, TGA) while some had additional defects (Table S1). Thus
02 low oxygen exposure perturbed cardiac OFT alignment development with maximum effect at E9.5.

04 **Alteration in cardiac outflow tract phenotype is apparent from E10.5**

05 To determine the developmental origin of the cardiac defects, we examined OFT morphology in embryos
06 exposed to 5.5% oxygen at E9.5 for 8 hours and then allowed to develop in normoxia for a further 16-24
07 hours. Control and exposed embryos were matched for somite number (range 33-38), and the OFT
08 myocardium visualized by wholemount myosin heavy chain (MHC) immunostaining. Optical projection
09 tomography (OPT) was used to make three-dimensional representations of the OFT myocardium (Figure
10 1A,B). The majority of exposed embryos had altered OFT morphology, with a shorter distal OFT and an
11 altered angle between proximal and distal OFT. There was a strong positive correlation between these
12 parameters for control embryos (Figure 1C, black points, $p=0.0086$), but not for exposed embryos (Figure
13 1C, red points, $p=0.3221$). Thus hypoxia-induced cardiac defects may result from a perturbation of distal
14 OFT formation.

16 **Low oxygen exposure affects proliferation in the second heart field**

17 The OFT forms primarily from cells of two embryonic lineages: cardiac progenitors of the second heart
18 field (SHF) and cardiac neural crest cells (CNC, reviewed in (Kelly, 2012; Neeb et al., 2013). Disruption
19 of SHF development can result in defective OFT elongation, alignment and/or septation. Such defects can
20 arise from activated apoptosis (Ilagan et al., 2006), premature differentiation (Liao et al., 2008) or
21 reduced cell proliferation (Xu et al., 2004; Ilagan et al., 2006). No apoptosis was detected by active/pro
22 Caspase 3 or TUNEL staining in the SHF, OFT or myocardium of control or exposed embryos (Figure
23 1D,E, Figure S1A-T). However increased numbers of apoptotic cells were present in the **neuroepithelium**
24 **of the posterior part of the neural tube**, otic vesicle and gut of exposed embryos, confirming that we were
25 able to detect apoptotic cells by these techniques (Figure S1A-T). Likewise, we did not detect any change
26 in expression levels or location of the myocyte differentiation marker MHC between control and exposed
27 embryos (Figure 1G,H). By contrast, there was a clear reduction in the extent of proliferation in the SHF,
28 OFT myocardium, branchial arch and forebrain in exposed embryos (Figure 1J-L, Figure S1U-C').
29 Quantification of the percentage of phosphorylated histone H3-positive nuclei indicated that proliferation
30 in the SHF and forebrain was more affected than that in the myocardium or branchial arch. Thus low
31 oxygen exposure results in a significant reduction of SHF cell proliferation, but does not induce apoptosis
32 or premature differentiation.

34 **Low oxygen exposure reduces FGF signaling in the second heart field**

35 We have shown that low oxygen exposure *in utero* reduces FGF signaling in the presomitic mesoderm
36 (PSM, Sparrow et al., 2012). In the SHF, reduction or loss of FGF signaling causes reduced cell

proliferation and OFT defects (Hutson et al., 2006; Park et al., 2006; Park et al., 2008; Zhang et al., 2008). We therefore examined the expression of direct target genes of FGF signaling in the SHF. *Spry1*, *Spry2* and *Spry4* transcripts in the SHF were significantly reduced after 8 hours exposure in the SHF (Figure 2A-C, and Figure S2N-Q). To gauge the dynamics of FGF signaling disruption, we exposed embryos for 1, 2, 4 or 8 hours to 5.5% oxygen and examined *Spry2* transcript levels. The significant reduction in transcript levels in the SHF was only observed in embryos exposed for 8 hours (Figure S2A-F). We next examined a more upstream component of FGF signal transduction. Depending on cellular context, FGF signal transduction can occur through three pathways: MAPK (ERK), AKT and PKC γ (Dorey and Amaya, 2010). ERK is the main pathway used by the cells of the SHF (Ilagan et al., 2006; Zhang et al., 2008). Phosphorylated-ERK1/2 was significantly reduced in the SHF after 8 hours exposure (Figure 2D-F). To investigate the dynamics of phosphorylated-ERK1/2 loss, levels were examined after 0.5, 1, 2, 4 or 8 hours exposure (Figure S2G-M). As little as 1 hours exposure caused a significant loss of phosphorylated-ERK1/2. Thus the reduced proliferation in SHF cardiac progenitor cells is likely to be due to reduced FGF signaling, and this occurs extremely rapidly upon exposure to hypoxia.

51

52 **Low oxygen exposure reduces FGFR1 levels in the second heart field**

There are many ways by which hypoxia might perturb FGF signaling. The simplest model is that receptor or ligand levels are reduced directly in response to cellular hypoxia. FGF signaling in the SHF involves the ligands FGF8 (Brown et al., 2004; Ilagan et al., 2006; Park et al., 2006) and FGF10 (Marguerie et al., 2006; Watanabe et al., 2010) and the receptors FGFR1 and FGFR2 (Marguerie et al., 2006; Park et al., 2008; Zhang et al., 2008). We focused on FGF8 and FGFR1, as these are prominent in SHF formation (Marguerie et al., 2006; Park et al., 2008; Watanabe et al., 2010). Levels of *Fgf8* transcripts were significantly reduced in the SHF from 4 hours exposure, but not after shorter exposures (Figure 3A-C, Figure S3A-F). Thus *Fgf8* transcript levels were not reduced until well after phosphorylated-ERK1/2 levels were significantly reduced (4 hours compared with 0.5 hours). This suggests that the *Fgf8* gene may itself be a target of FGF signaling, and that its reduced transcription is a consequence rather than the cause of reduced FGF signaling. This is supported by the observation that conditional knockout of FGFR1 in the midbrain–hindbrain boundary greatly reduces FGF signaling and abolishes *Fgf8* expression (Jukkola et al., 2006). We next examined FGFR1 protein expression. In control embryos, FGFR1 protein was concentrated in perinuclear cytoplasmic puncta with lower levels of background staining throughout the cell (Figure 3D). This is consistent with observations in different cell types *in vivo* and *in vitro* (Prudovsky et al., 1994; Ozaki et al., 2000). The puncta co-stained with the *cis*-Golgi protein GM130 (Figure 3E,F). By contrast, after 8 hours exposure there was a reduction in both total FGFR1 (7/10 embryos, Figure 3G) and Golgi-localized FGFR1 (8/10 embryos, Figure 3K). Concomitantly, Golgi sub-cellular localization did not appear to be affected (Figure 3E,F,I,J). Low oxygen exposure had a rapid effect on FGFR1 protein expression, with exposure for as little as 1 hours resulting in a significant loss of

73 Golgi-localized FGFR1 protein and total FGFR1 significantly reduced after 4 hours exposure (Figure
74 S3G-T). We confirmed this reduction by immunoblot of whole embryo extracts (Figure 3O, Figure
75 S3B'). To assess the specificity of FGFR1 loss, we examined the protein expression of another receptor
76 tyrosine kinase expressed in the SHF, PDGFR β . PDGFR β protein was present throughout the cytoplasm
77 and plasma membrane of SHF cells at equivalent levels in control and exposed embryos (Figure 3L-N
78 and Figure S3U-A'). Thus FGFR1 protein levels are rapidly reduced in the SHF in response to low
79 oxygen exposure, and there is some specificity to this response.

80

81 **SHF cells in embryos exposed to lowered oxygen levels *in utero* are hypoxic**

82 We next investigated how hypoxia causes FGFR1 protein loss. Maternal low oxygen exposure is likely to
83 have many effects on the embryo. Previously we have shown that the embryonic myocardium is
84 particularly susceptible to low oxygen exposure (O'Reilly et al., 2014). We therefore investigated whether
85 the SHF was similarly affected. We measured embryonic cellular oxygen levels using the compound
86 HypoxyprobeTM (Raleigh et al., 1999). Pregnant mice were injected with HypoxyprobeTM, and then
87 exposed to 5.5% oxygen for 3 hours. Limited staining was detected in control embryos under these
88 conditions (Figure 4A-B). By contrast, there was strong staining throughout exposed embryos, including
89 the SHF (Figure 4C-D). The response to cellular hypoxia in mammalian embryos is mediated by the
90 hypoxia inducible factor (HIF1, reviewed in (Dunwoodie, 2009). The HIF1 α subunit of this transcription
91 factor is rapidly degraded in normoxia (Wang et al., 1995), but it is stabilized and transported to the
92 nucleus when cellular oxygen levels fall below 2% (Jiang et al., 1996). Nuclear HIF1 α staining was
93 detected in the myocardium of embryos after as little as 0.5 hours exposure (Figure 4E,F,H. Figure S4A-
94 H,M and (O'Reilly et al., 2014). Nuclear staining was also visible in the gut (Figure S4N). No nuclear
95 staining of HIF1 α was visible in the SHF of embryos exposed to low oxygen (Figure 4E,F,G), despite
96 these cells being hypoxic, although there was a slight increase in the total amount of HIF1 α staining.

97

98 **SHF cells in embryos exposed to lowered oxygen levels *in utero* induce the unfolded protein 99 response**

00 One cellular consequence of hypoxia is disruption of protein folding in the endoplasmic reticulum (ER,
01 (Feldman et al., 2005). If such disruption is severe, the unfolded protein response (UPR) will be induced.
02 This is a coordinated cellular program that reduces the rate of protein synthesis generally, increases the
03 expression of molecular chaperones to assist protein refolding, upregulates the ER-associated degradation
04 (ERAD) pathway to degrade terminally misfolded proteins, and induces apoptosis if ER stress persists
05 (Kitamura, 2013). We examined expression of a late marker of the UPR, DNA-damage-inducible
06 transcript 3 (DDIT3, also known as CHOP) to determine if the UPR was induced in low oxygen exposed
07 embryos. DDIT3 was robustly induced in the SHF of 8/12 embryos after 8 hours exposure, and in a
08 subset of exposed embryos from as early as 2 hours (Figure 4I-K, Figure S4O-U). We also analyzed the

09 production of an immediate early marker of the UPR, the splicing of the *Xbp1* transcript. Significant
10 levels of spliced *Xbp1* were detectable by qPCR in whole embryo RNA extracts after as little as 0.5 hours
11 exposure (Figure 4L). This suggests that the UPR is rapidly induced in embryos exposed to low oxygen
12 levels. Thus the specific loss of FGFR1 protein expression in embryos exposed to low oxygen levels
13 correlates with both hypoxia and induction of the UPR in the SHF.

15 **FGFR1 protein levels are reduced *in vitro* in response to hypoxia and other cellular stressors**

16 We next developed an *in vitro* model system to investigate the molecular mechanism by which FGFR1 is
17 lost in response to hypoxia. We used mouse muscle satellite C2C12 cells because they express FGFR1
18 and can activate the FGF pathway through ERK (Erck et al., 1998). Cells were cultured for 1-4 hours in
19 0.1% oxygen and then protein extracts analyzed by immunoblot (Figure 5A,B). In keeping with our *in*
20 *vivo* results, levels of FGFR1 and phosphorylated-ERK1/2 were significantly reduced by hypoxia whilst
21 total ERK1/2 and β -tubulin levels remained constant. The degree of reduction was similar to that
22 observed in immunoblots of whole embryos exposed to 5.5% oxygen for 1-4 hours (Figure 3O). Exposed
23 cells also had significantly increased levels of the translation initiation factor phosphorylated-eIF2 α and
24 DDIT3, indicating robust UPR activation (Figure 5A,B). We also tested the effects of other UPR-
25 inducing stressors on FGFR1 stability *in vitro*. Short term treatment of cells with hydrogen peroxide,
26 increased temperature, or high pH all reduced FGFR1 protein levels by a similar extent to hypoxic
27 treatment (Figure S5A-C). Phosphorylated-eIF2 α was induced in all cases, confirming UPR activation
28 (data not shown). Thus other cellular stressors that induce the UPR, including increased reactive oxygen
29 species or hyperthermia, also result in reduced FGFR1 protein levels *in vitro*.

31 **FGFR1 protein levels are reduced *in vitro* and *in vivo* due to UPR-triggered translation inhibition**

32 The UPR involves three separate signaling pathways mediated by IRE1, PERK and ATF6 respectively.
33 We next investigated if the reduction of FGFR1 protein levels *in vitro* was due to the action of one
34 particular pathway. The UPR activates the IRE1 pathway via *Xbp1* transcript splicing enabling translation
35 of this transcription factor, increasing expression of chaperones and activating degradation of misfolded
36 proteins. We compared FGFR1 protein levels in hypoxic cells with- or without treatment with a small
37 molecule inhibitor of IRE1, 4-methyl umbelliferone 8-carbaldehyde (4 μ 8c, (Cross et al., 2012). Hypoxia
38 caused a significant reduction in FGFR1 protein levels, and treatment with 4 μ 8c did not alter this
39 response (Figure 6A). To confirm the efficacy of 4 μ 8c treatment, we monitored *Xbp1* splicing levels
40 using the transiently transfected FLAG-XBP1 Δ DBD-venus reporter (Iwawaki et al., 2004). As expected,
41 hypoxia activated *Xbp1* splicing, and treatment with 4 μ 8c under hypoxic conditions prevented *Xbp1*
42 splicing (Figure 6B). We also confirmed the specificity of 4 μ 8c action, as induced levels of
43 phosphorylated-eIF2 α and DDIT3 under hypoxic conditions were unaffected by 4 μ 8c treatment (Figure
44 6C,D). The UPR also causes a global reduction in cap-dependent translation. This process is controlled by

45 activation of the serine-threonine kinase PERK, which phosphorylates and inactivates the translational
46 initiation factor eIF2 α (Kitamura, 2013). We compared FGFR1 and phosphorylated-ERK1/2 protein
47 levels in hypoxic cells with- or without treatment with an inhibitor of PERK (GSK2606414, (Axten et al.,
48 2012) Figure 6E,F). As above, we confirmed inhibitor activity and specificity by monitoring
49 phosphorylated-eIF2 α and DDIT3 levels (Figure 6G,H). Strikingly, treatment with GSK2606414 rescued
50 the reduction in FGFR1 levels induced by hypoxia. This rescue of FGFR1 levels did not result in
51 sustained phosphorylated-ERK1/2. Three FGFR1 bands, with different degrees of glycosylation, were
52 detected by immunoblotting (Figure 6I). The highest molecular weight band (140kDa), resistant to
53 Endoglycosidase H (EndoH) digestion, represents the mature form of FGFR1 (Figure S5D; (Koika et al.,
54 2013). Whilst total FGFR1 levels were rescued by GSK2606414 treatment (Figure 6E), levels of the
55 mature form of the receptor increased to a lesser extent than the immature forms (Figure 6I,J,K). The
56 abnormal build-up of the immature forms suggests that receptor maturation is disrupted by hypoxia,
57 providing an explanation for why phosphorylated-ERK1/2 levels were not rescued (Figure 6F). We next
58 sought to confirm that FGFR1 levels could be rescued by inhibiting PERK in embryos exposed to
59 hypoxia (Figure 6L-O). We treated pregnant C57BL/6J mice on E9.5 with a single dose of GSK2606414
60 by oral gavage 1 hour before exposure to 5.5% oxygen for 2 hours. As before, low oxygen exposure
61 without GSK2606414 treatment resulted in a significant loss of both total- and Golgi-localized FGFR1
62 protein and, importantly, treatment with GSK2606414 rescued the hypoxia-induced reduction in FGFR1
63 in the SHF (Figure 6T,U). Consistent with our *in vitro* findings, phospho-ERK1/2 levels were not
64 sustained in the SHF despite normal FGFR1 levels (Figure 6P-S,V). These data indicate that inhibition of
65 FGFR1 protein levels in response to hypoxia occurs specifically by PERK-induced inhibition of
66 translation, both *in vitro* and *in vivo*. PERK inhibition restored FGFR1 levels generally, but not the
67 mature active form of FGFR1 and consequently not signaling via phospho-ERK1/2.

68

69 DISCUSSION

70 Almost two hundred years ago, Étienne Geoffroy Saint Hilaire showed that gestational hypoxia disrupts
71 embryonic development (Geoffroy Saint Hilaire, 1820). The cellular and molecular consequences of this
72 finding are only now being elucidated. We have previously shown that short-term gestational hypoxia
73 disrupts FGF signaling in the presomitic mesoderm (PSM), altering somitogenesis and leading to
74 vertebral defects (Sparrow et al., 2012). Here we extend this study by demonstrating that short-term
75 gestational hypoxia causes abnormal heart development, resulting in heart defects that are the most
76 common subtype of human congenital heart disease (CHD). Interestingly we observed an almost bimodal
77 response to hypoxia, with only about ~50% of embryos developing heart defects after hypoxic exposure.
78 This supports the notion that some variation in clinical outcome of human cases of CHD is environmental
79 in nature. The defects induced by hypoxia are consistent with impaired function of a progenitor

80 population of the heart, the second heart field (SHF). Accordingly, we show that hypoxia reduces FGFR1
81 protein levels and FGF signaling in the SHF, and also activates the unfolded protein response (UPR). In
82 both cultured cells and *in vivo*, we identify that the reduced levels of FGFR1 are likely caused by one
83 specific function of the UPR: inhibition of cap-dependent translation. However, it should be noted that we
84 were not able to test if the third UPR pathway (mediated by ATF6) was also involved. We suggest a
85 model in which the hypoxia-induced UPR results in reduced FGF signaling in the SHF, disrupting heart
86 development and leading to morphological heart defects. We propose that other stressors that trigger the
87 UPR during embryogenesis, such as increased reactive oxygen species or hyperthermia, may also cause
88 CHD. In addition, UPR activation by such stressors may also occur in sites in addition to the SHF. This
89 suggests that activation of the UPR might be a more general disruptor of embryogenesis and thus cause a
90 range of birth defects.

91 Cells respond to stresses in a variety of ways, of which the UPR is only one. It is formally possible
92 that other cellular stress responses are activated by hypoxia such as the mTOR pathway (Wouters and
93 Koritzinsky, 2008) and the nucleolar stress response (Boulon et al., 2010) (James et al., 2014). The effects
94 of these pathways on heart development could be assessed in future studies.

95 The hypoxia-mediated induction of the UPR is reversible in our mouse model. This is evident from
96 the reiterative nature of somitogenesis, where each somite is independently formed temporally and
97 spatially. Thus somites formed after gestational hypoxia ceases are normal, and these give rise to normal
98 vertebrae (Sparrow et al., 2012). In contrast, transient activation of the UPR has lasting morphological
99 effects on the heart. This is because the final structure of the heart relies on many interdependent
00 processes during embryogenesis, with perturbation at any point disrupting its final structure. Thus,
01 although the UPR is reversible during embryogenesis, the effects on organ morphology can be enduring.

02 One of the early UPR responses is PERK-dependent attenuation of general protein synthesis.
03 Therefore, it might be expected that a short-term translation block would simply cause a temporary
04 reduction in embryo growth rate. However, the translation block appears to particularly affect the levels
05 of some proteins but not others. In doing so, it disrupts specific processes and leads to distinct
06 morphological defects. One explanation for this is that the UPR-induced translation block is specifically
07 affecting cellular processes that are reliant on a rapid replenishment of proteins. For example, FGFR1-
08 mediated signaling results in receptor degradation and for signaling to continue, more FGFR1 needs to be
09 translated (Haugsten et al., 2005). Thus FGFR1 cell surface replacement would be prevented by PERK-
10 induced translation inhibition. This is in contrast to FGFR4, where receptor recycling, rather than
11 degradation, occurs after activation. We might expect receptors of this type to be unaffected by
12 translation inhibition. Indeed, this may explain why protein expression levels of PDGFR β , another
13 receptor tyrosine kinase (RTK) expressed in the SHF like FGFR1, were not affected by hypoxia within
14 the experimental time frame. This differential effect of the UPR on receptor expression and function is an
15 important area for future investigation.

16 We show that the hypoxia-induced reduction of FGFR1 is due to activation of the UPR and the
17 PERK-dependent inhibition of translation. Inhibition of PERK rescued FGFR1 in cultured cells and *in*
18 *vivo*, but did not rescue the reduction of phosphorylated-ERK1/2. This can be explained by the fact that
19 although total FGFR1 levels are restored, the mature form of the receptor is significantly
20 underrepresented. This is not surprising, as although GSK2606414 relieves the inhibition of translation,
21 hypoxia would still inhibit protein folding and maturation in the ER and Golgi (Koritzinsky et al., 2013).

22 Potentially any stressor present during gestation that triggers UPR in a tissue where FGFR1 is
23 active could disrupt the FGF-dependent developmental processes and lead to birth defects. Accordingly,
24 our studies show that gestational hypoxia at E9.5 in mouse disrupts FGF signaling in the precursor tissues
25 of the heart and vertebrae leading to defects in these structures (this study and (Sparrow et al., 2012). The
26 development of other organs might well be disrupted, as FGF/FGFR1 signaling has many key roles in
27 embryogenesis (Thisse and Thisse, 2005; Itoh and Ornitz, 2011). More broadly, our findings suggest that
28 any gestational stress that activates the UPR could disrupt any number of developmental processes and
29 lead to birth defects. The types and numbers of defects that arise will be affected by the timing, duration
30 and degree of the stress during embryogenesis, and the robustness of developmental processes to
31 withstand perturbation. In humans, different types of birth defects can arise with a non-random co-
32 occurrence. For example, patients with a spectrum of various combinations of Vertebral anomalies, Anal
33 atresia, Cardiac defects, Tracheoesophageal fistula and/or Esophageal atresia, Renal & Radial anomalies
34 and Limb defects may be classified as having VACTERL association (OMIM 192350;). It is possible that
35 the critical stages of development of these organs are coincident. If so, activation of the UPR during this
36 stage of embryogenesis may result in VACTERL.

37 How likely is it that the UPR is triggered during gestation? In addition to hypoxia, the UPR is
38 activated in response to a variety of environmental stressors such as pollution and pathological conditions
39 including maternal diabetes, viral infection and hyperthermia (Kitamura, 2013). Strikingly, many of these
40 are identified as environmental risk factors for causing congenital malformation in humans (Jenkins et al.,
41 2007). For example, offspring of mothers with pre-gestational diabetes have a significantly increased risk
42 of congenital heart disease with a relative risk of 3-18 (Jenkins et al., 2007), and the embryos of diabetic
43 mice show significant activation of the UPR (Zhao, 2012). In addition, stressors such as hyperthermia and
44 hypoxemia are both associated with increased risk of birth defects in humans (Jenkins et al., 2007), and
45 activation of the UPR in cell culture (Kitamura, 2013). Thus our results may provide a mechanism for the
46 induction of birth defects by a wide array of environmental factors.

47 Finally, our *in vitro* system could be used as the basis of a high-throughput screening strategy to
48 identify potential prophylactic agents to reduce the risks of congenital heart disease, following the
49 folate/neural tube defect paradigm (MRC Vitamin Study Research Group, 1991). Such prophylactic
50 agents could then be validated in our *in vivo* system. This has an encouraging precedent, as oral treatment
51 targeting the UPR abrogates development of clinical prion disease in mice (Moreno et al., 2013). Such an

52 approach could have the potential to significantly reduce the incidence of human congenital defects.

53

54 **MATERIALS AND METHODS**

55 **Animal experiments**

56 All animal experiments were performed in accordance with the protocols approved by the Garvan
57 Institute of Medical Research/St Vincent's Animal Experimentation Ethics Committee, Sydney, Australia
58 (approval 12/33). **C57BL6/J dams and sires were mated.** Pregnant mice were exposed to lowered oxygen
59 levels at normal atmospheric pressure as described (Sparrow et al., 2012). After exposure the mice were
60 either sacrificed and embryos harvested, or mice were returned to normoxia for embryo harvest at a later
61 date. For GSK2606414 experiments, pregnant mice were dosed with 50 mg/kg by oral gavage on E9.5, 1
62 hour prior to hypoxic exposure. The dose was previously shown to effectively prevent UPR-mediated
63 translational repression *in vivo* (Moreno et al., 2013).

64

65 **Heart morphology determination**

66 Heart morphology was determined using paraffin sectioning or magnetic resonance imaging (MRI) as
67 previously described (O'Reilly et al., 2014), or by optical projection tomography (OPT) as described in
68 the Supplementary Materials and Methods. Heart morphology for all samples was assessed by the same
69 observer, with classification of heart defects confirmed by an independent person.

70

71 **TUNEL staining and immunohistochemistry**

72 Paraffin sections were labeled with digoxigenin-nucleotide using the ApopTag® Fluorescein In Situ
73 Apoptosis Detection Kit (Abcam). Labeled DNA fragments were detected by anti-digoxigenin-AP, Fab
74 fragments (Roche Life Sciences) and NBT/BCIP solution (Roche Life Sciences). We performed whole-
75 mount immunofluorescence on fixed embryos as previously described (Geffers et al., 2007). For details
76 concerning immunohistochemistry see Supplementary Materials and Methods.

77

78 **RNA *in situ* hybridization**

79 We performed RNA wholemount *in situ* hybridization as described previously (Dunwoodie et al., 1997),
80 with probes listed in the Supplementary Materials and Methods.

81

82 **Quantitative RT-PCR**

83 Levels of spliced and unspliced *Xbp1* transcripts in RNA extracts from whole E9.5 embryos were
84 determined using custom TaqMan® gene expression assays (Applied Biosystems) designed using
85 published sequences (Hayashi et al., 2007). RNA extraction, reverse transcription and qPCR were
86 performed as previously described (O'Reilly et al., 2014).

87

88 **Cell culture and immunoblots**

89 Mouse muscle satellite C2C12 cells were cultured in low oxygen using a H35 Hypoxystation (Don
90 Whitley Scientific). Culture medium was equilibrated in 0.1% O₂ overnight prior to use. Culture dishes
91 were transferred to the workstation, rinsed once with hypoxia-equilibrated medium, and incubated in
92 fresh hypoxia-equilibrated medium for the indicated times. For the study of UPR inhibitors, cells were
93 incubated for 2 hours in the normoxic or hypoxia-equilibrated medium containing inhibitor. For detection
94 of *Xbp1* splicing in the 4μ8c experiments, a plasmid encoding FLAG®-tagged XBP1ΔDBD-venus
95 (Iwawaki et al., 2004) was transiently transfected into C2C12 cells using Lipofectamine® LTX and
96 PLUS™ reagent (Life Technologies) 24 hours prior to hypoxic exposure. For further details see
97 Supplementary Materials and Methods.

98

99 **Statistical analyses**

00 All statistical analyses were performed with Prism 6 (GraphPad Software Inc). Gene and protein staining
01 intensity from RNA wholemount *in situ* hybridizations, immunohistochemistry and immunoblot
02 experiments were compared using Kruskal-Wallis one-way ANOVA with Dunnett's *post hoc* test to
03 compare all treatment groups with the control, except for the data in Figure 4L and 6A-J, which were
04 tested with ANOVA followed by Tukey's *post hoc* test to compare the means of each group with every
05 other group. The linear correlation between distal OFT length and inner angle between proximal and
06 distal OFT (Figure 1) was tested using non-parametric Spearman correlation. The statistical significance
07 of the prevalence of heart defects or resorbed embryos in exposed versus unexposed embryos (Table 1)
08 was tested using a one-tailed Fisher's exact test. In Figures, data were presented as mean ± standard
09 deviation with p values indicated as the number of stars (* p<0.05, ** p<0.01, *** p<0.001, ****
10 p<0.0001).

11

12 **ACKNOWLEDGMENTS**

13 We thank G. Martin, I. Mason and M. Muira for plasmids; BioCORE staff and Y. Wang for technical
14 assistance; G. Maghzal for technical and intellectual assistance; Herbert Smith for donating the confocal
15 microscopes and Chain Reaction for donating the OPT, used in this study.

16 **COMPETING INTERESTS**

17 No competing interests declared

19 **AUTHOR CONTRIBUTIONS**

20 HS, VCO, JLMM, TRB, MXY, BEC, SMG, GC, DBS performed experiments

21 HS, VCO, JLMM, TRB, MXY, GC, DBS, RS, SLD analysed data

22 HS, RS, RMG, GC, DBS, SLD wrote the manuscript

23 SMG, RS, RMG, DBS, SLD secured funding

24 SLD conceived the study and is responsible for all aspects of this research and its communication.

26 **FUNDING**

27 This research was supported by National Health and Medical Research Council (NHMRC) project grant
28 APP1019776 (SLD, DBS, SMG); NHMRC program grant 1074386 (SLD, RMG); NHMRC Senior
29 Research Fellowship 1042002 (SLD); Chain Reaction (The Ultimate Corporate Bike Challenge) and the
30 Office of Health and Medical Research, NSW State Government (RMG, SLD, RS).

32 **REFERENCES**

34 Abu-Issa, R., Smyth, G., Smoak, I., Yamamura, K. and Meyers, E. N. (2002) 'Fgf8 is required for
35 pharyngeal arch and cardiovascular development in the mouse', *Development* 129(19): 4613-25.

37 Allan, V.J. (1999) *Protein Localization by Fluorescence Microscopy*, Oxford, United Kingdom: Oxford
38 University Press.

40 Andersen, T. A., Troelsen Kde, L. and Larsen, L. A. (2014) 'Of mice and men: molecular genetics of
41 congenital heart disease', *Cell Mol Life Sci* 71(8): 1327-52.

43 Axten, J. M., Medina, J. R., Feng, Y., Shu, A., Romeril, S. P., Grant, S. W., Li, W. H., Heerding, D. A.,
44 Minthorn, E., Mencken, T. et al. (2012) 'Discovery of 7-methyl-5-(1-{[3-(trifluoromethyl)phenyl]acetyl}-
45 2,3-dihydro-1H-indol-5-yl)-7H-pyrrolo[2,3-d]pyrimidin-4-amine (GSK2606414), a potent and selective
46 first-in-class inhibitor of protein kinase R (PKR)-like endoplasmic reticulum kinase (PERK)', *J Med*
47 *Chem* 55(16): 7193-207.

49 Benson, D. W., Silberbach, G. M., Kavanaugh-McHugh, A., Cottrill, C., Zhang, Y., Riggs, S., Smalls, O.,
50 Johnson, M. C., Watson, M. S., Seidman, J. G. et al. (1999) 'Mutations in the cardiac transcription factor
51 NKX2.5 affect diverse cardiac developmental pathways', *J Clin Invest* 104(11): 1567-73.
52
53 Blue, G. M., Kirk, E. P., Sholler, G. F., Harvey, R. P. and Winlaw, D. S. (2012) 'Congenital heart disease:
54 current knowledge about causes and inheritance', *Med J Aust* 197(3): 155-9.
55
56 Boulon, S., Westman, B. J., Hutten, S., Boisvert, F. M. and Lamond, A. I. (2010) 'The nucleolus under
57 stress', *Mol Cell* 40(2): 216-27.
58
59 Brown, C. B., Wenning, J. M., Lu, M. M., Epstein, D. J., Meyers, E. N. and Epstein, J. A. (2004) 'Cre-
60 mediated excision of Fgf8 in the Tbx1 expression domain reveals a critical role for Fgf8 in cardiovascular
61 development in the mouse', *Dev Biol* 267(1): 190-202.
62
63 Bruneau, B. G. (2008) 'The developmental genetics of congenital heart disease', *Nature* 451(7181): 943-8.
64 Cross, B. C., Bond, P. J., Sadowski, P. G., Jha, B. K., Zak, J., Goodman, J. M., Silverman, R. H.,
65 Neubert, T. A., Baxendale, I. R., Ron, D. et al. (2012) 'The molecular basis for selective inhibition of
66 unconventional mRNA splicing by an IRE1-binding small molecule', *Proc Natl Acad Sci U S A* 109(15):
67 E869-78.
68
69 Dorey, K. and Amaya, E. (2010) 'FGF signalling: diverse roles during early vertebrate embryogenesis',
70 *Development* 137(22): 3731-42.
71
72 Dunwoodie, S. L. (2009) 'The role of hypoxia in development of the Mammalian embryo', *Dev Cell*
73 17(6): 755-73.
74
75 Dunwoodie, S. L., Henrique, D., Harrison, S. M. and Beddington, R. S. (1997) 'Mouse Dll3: a novel
76 divergent Delta gene which may complement the function of other Delta homologues during early pattern
77 formation in the mouse embryo', *Development* 124(16): 3065-76.
78
79 Erck, C., Meisinger, C., Grothe, C. and Seidl, K. (1998) 'Regulation of nerve growth factor and its low-
80 affinity receptor (p75NTR) during myogenic differentiation', *J Cell Physiol* 176(1): 22-31.
81
82 Fahed, A. C., Gelb, B. D., Seidman, J. G. and Seidman, C. E. (2013) 'Genetics of congenital heart
83 disease: the glass half empty', *Circ Res* 112(4): 707-20.
84
85 Feldman, D. E., Chauhan, V. and Koong, A. C. (2005) 'The unfolded protein response: a novel
86 component of the hypoxic stress response in tumors', *Mol Cancer Res* 3(11): 597-605.
87
88 Geoffroy Saint Hilaire, E. (1820) 'Différents états de pesanteur des oeufs au commencement et a la fin de
89 l'incubation', *Journal Complémentaire des Sciences Medicales* 7: 271.
90
91 Haugsten, E. M., Sorensen, V., Brech, A., Olsnes, S. and Wesche, J. (2005) 'Different intracellular
92 trafficking of FGF1 endocytosed by the four homologous FGF receptors', *J Cell Sci* 118(Pt 17): 3869-81.
93
94 Hayashi, A., Kasahara, T., Iwamoto, K., Ishiwata, M., Kametani, M., Kakiuchi, C., Furuichi, T. and Kato,
95 T. (2007) 'The role of brain-derived neurotrophic factor (BDNF)-induced XBP1 splicing during brain
96 development', *J Biol Chem* 282(47): 34525-34.
97
98 Hutson, M. R., Zhang, P., Stadt, H. A., Sato, A. K., Li, Y. X., Burch, J., Creazzo, T. L. and Kirby, M. L.
99 (2006) 'Cardiac arterial pole alignment is sensitive to FGF8 signaling in the pharynx', *Dev Biol* 295(2):
00 486-97.
01

02 Ilagan, R., Abu-Issa, R., Brown, D., Yang, Y. P., Jiao, K., Schwartz, R. J., Klingensmith, J. and Meyers,
03 E. N. (2006) 'Fgf8 is required for anterior heart field development', *Development* 133(12): 2435-45.
04

05 Ingalls, T. H., Curley, F. J. and Prindle, R. A. (1952) 'Experimental production of congenital anomalies;
06 timing and degree of anoxia as factors causing fetal deaths and congenital anomalies in the mouse', *N*
07 *Engl J Med* 247(20): 758-68.
08

09 Itoh, N. and Ornitz, D. M. (2011) 'Fibroblast growth factors: from molecular evolution to roles in
10 development, metabolism and disease', *J Biochem* 149(2): 121-30.
11

12 Iwawaki, T., Akai, R., Kohno, K. and Miura, M. (2004) 'A transgenic mouse model for monitoring
13 endoplasmic reticulum stress', *Nat Med* 10(1): 98-102.
14

15 James, A., Wang, Y., Raje, H., Rosby, R. and DiMario, P. (2014) 'Nucleolar stress with and without p53',
16 *Nucleus* 5(5): 402-26.
17

18 Jenkins, K. J., Correa, A., Feinstein, J. A., Botto, L., Britt, A. E., Daniels, S. R., Elixson, M., Warnes, C.
19 A., Webb, C. L. and American Heart Association Council on Cardiovascular Disease in the, Young
20 (2007) 'Noninherited risk factors and congenital cardiovascular defects: current knowledge: a scientific
21 statement from the American Heart Association Council on Cardiovascular Disease in the Young:
22 endorsed by the American Academy of Pediatrics', *Circulation* 115(23): 2995-3014.
23

24 Jiang, B. H., Semenza, G. L., Bauer, C. and Marti, H. H. (1996) 'Hypoxia-inducible factor 1 levels vary
25 exponentially over a physiologically relevant range of O₂ tension', *Am J Physiol* 271(4 Pt 1): C1172-80.
26

27 Jukkola, T., Lahti, L., Naserke, T., Wurst, W. and Partanen, J. (2006) 'FGF regulated gene-expression and
28 neuronal differentiation in the developing midbrain-hindbrain region', *Dev Biol* 297(1): 141-57.
29

30 Kelly, R. G. (2012) 'The second heart field', *Curr Top Dev Biol* 100: 33-65.
31

32 Kitamura, M. (2013) 'The unfolded protein response triggered by environmental factors', *Semin*
33 *Immunopathol* 35(3): 259-75.
34

35 Koika, V., Varnavas, P., Valavani, H., Sidis, Y., Plummer, L., Dwyer, A., Quinton, R., Kanaka-
36 Gantenbein, C., Pitteloud, N., Sertedaki, A. et al. (2013) 'Comparative functional analysis of two
37 fibroblast growth factor receptor 1 (FGFR1) mutations affecting the same residue (R254W and R254Q) in
38 isolated hypogonadotropic hypogonadism (IHH)', *Gene* 516(1): 146-51.
39

40 Koritzinsky, M., Levitin, F., van den Beucken, T., Rumantir, R. A., Harding, N. J., Chu, K. C., Boutros,
41 P. C., Braakman, I. and Wouters, B. G. (2013) 'Two phases of disulfide bond formation have differing
42 requirements for oxygen', *J Cell Biol* 203(4): 615-27.
43

44 Liao, J., Aggarwal, V. S., Nowotschin, S., Bondarev, A., Lipner, S. and Morrow, B. E. (2008)
45 'Identification of downstream genetic pathways of Tbx1 in the second heart field', *Dev Biol* 316(2): 524-
46 537.
47

48 Marguerie, A., Bajolle, F., Zaffran, S., Brown, N. A., Dickson, C., Buckingham, M. E. and Kelly, R. G.
49 (2006) 'Congenital heart defects in Fgfr2-IIIb and Fgf10 mutant mice', *Cardiovasc Res* 71(1): 50-60.
50

51 Miquerol, L. and Kelly, R. G. (2013) 'Organogenesis of the vertebrate heart', *Wiley Interdiscip Rev Dev*
52 *Biol* 2(1): 17-29.
53

54 Moreau, J. L., Artap, S. T., Shi, H., Chapman, G., Leone, G., Sparrow, D. B. and Dunwoodie, S. L.
55 (2014) 'Cited2 is required in trophoblasts for correct placental capillary patterning', *Dev Biol* 392(1): 62-
56 79.

57

58 Moreno, J. A., Halliday, M., Molloy, C., Radford, H., Verity, N., Axten, J. M., Ortori, C. A., Willis, A.
59 E., Fischer, P. M., Barrett, D. A. et al. (2013) 'Oral treatment targeting the unfolded protein response
60 prevents neurodegeneration and clinical disease in prion-infected mice', *Sci Transl Med* 5(206):
61 206ra138.

62

63 Neeb, Z., Lajiness, J. D., Bolanis, E. and Conway, S. J. (2013) 'Cardiac outflow tract anomalies', *Wiley*
64 *Interdiscip Rev Dev Biol* 2(4): 499-530.

65

66 O'Reilly, V. C., Lopes Floro, K., Shi, H., Chapman, B. E., Preis, J. I., James, A. C., Chapman, G.,
67 Harvey, R. P., Johnson, R. S., Grieve, S. M. et al. (2014) 'Gene-environment interaction demonstrates the
68 vulnerability of the embryonic heart', *Dev Biol* 391(1): 99-110.

69

70 Ornoy, A., Reece, E. A., Pavlinkova, G., Kappen, C. and Miller, R. K. (2015) 'Effect of maternal diabetes
71 on the embryo, fetus, and children: congenital anomalies, genetic and epigenetic changes and
72 developmental outcomes', *Birth Defects Res C Embryo Today* 105(1): 53-72.

73

74 Ozaki, S., Radeke, M. J. and Anderson, D. H. (2000) 'Rapid upregulation of fibroblast growth factor
75 receptor 1 (flg) by rat photoreceptor cells after injury', *Invest Ophthalmol Vis Sci* 41(2): 568-79.

76

77 Park, E. J., Ogden, L. A., Talbot, A., Evans, S., Cai, C. L., Black, B. L., Frank, D. U. and Moon, A. M.
78 (2006) 'Required, tissue-specific roles for Fgf8 in outflow tract formation and remodeling', *Development*
79 133(12): 2419-33.

80

81 Park, E. J., Watanabe, Y., Smyth, G., Miyagawa-Tomita, S., Meyers, E., Klingensmith, J., Camenisch, T.,
82 Buckingham, M. and Moon, A. M. (2008) 'An FGF autocrine loop initiated in second heart field
83 mesoderm regulates morphogenesis at the arterial pole of the heart', *Development* 135(21): 3599-610.

84

85 Prudovsky, I., Savion, N., Zhan, X., Friesel, R., Xu, J., Hou, J., McKeehan, W. L. and Maciag, T. (1994)
86 'Intact and functional fibroblast growth factor (FGF) receptor-1 trafficks near the nucleus in response to
87 FGF-1', *J Biol Chem* 269(50): 31720-4.

88

89 Raleigh, J. A., Chou, S. C., Arteel, G. E. and Horsman, M. R. (1999) 'Comparisons among pimonidazole
90 binding, oxygen electrode measurements, and radiation response in C3H mouse tumors', *Radiat Res*
91 151(5): 580-9.

92

93 Ramakrishnan, A., Lee, L. J., Mitchell, L. E. and Agopian, A. J. (2015) 'Maternal Hypertension During
94 Pregnancy and the Risk of Congenital Heart Defects in Offspring: A Systematic Review and Meta-
95 analysis', *Pediatr Cardiol* 36(7): 1442-1451.

96

97 Schott, J. J., Benson, D. W., Basson, C. T., Pease, W., Silberbach, G. M., Moak, J. P., Maron, B. J.,
98 Seidman, C. E. and Seidman, J. G. (1998) 'Congenital heart disease caused by mutations in the
99 transcription factor NKX2-5', *Science* 281(5373): 108-11.

00

01 Sparrow, D. B., Chapman, G., Smith, A. J., Mattar, M. Z., Major, J. A., O'Reilly, V. C., Saga, Y., Zackai,
02 E. H., Dormans, J. P., Alman, B. A. et al. (2012) 'A mechanism for gene-environment interaction in the
03 etiology of congenital scoliosis', *Cell* 149(2): 295-306.

04

05 Sullivan, P. M., Dervan, L. A., Reiger, S., Buddhe, S. and Schwartz, S. M. (2015) 'Risk of congenital
06 heart defects in the offspring of smoking mothers: a population-based study', *J Pediatr* 166(4): 978-984
07 e2.

- Thisse, B. and Thisse, C. (2005) 'Functions and regulations of fibroblast growth factor signaling during embryonic development', *Dev Biol* 287(2): 390-402.
- Thom, T., Haase, N., Rosamond, W., Howard, V. J., Rumsfeld, J., Manolio, T., Zheng, Z. J., Flegal, K., O'Donnell, C., Kittner, S. et al. (2006) 'Heart disease and stroke statistics--2006 update: a report from the American Heart Association Statistics Committee and Stroke Statistics Subcommittee', *Circulation* 113(6): e85-151.
- van der Linde, D., Konings, E. E., Slager, M. A., Witsenburg, M., Helbing, W. A., Takkenberg, J. J. and Roos-Hesselink, J. W. (2011) 'Birth prevalence of congenital heart disease worldwide: a systematic review and meta-analysis', *J Am Coll Cardiol* 58(21): 2241-7.
- Wang, G. L., Jiang, B. H., Rue, E. A. and Semenza, G. L. (1995) 'Hypoxia-inducible factor 1 is a basic-helix-loop-helix-PAS heterodimer regulated by cellular O₂ tension', *Proc Natl Acad Sci U S A* 92(12): 5510-4.
- Watanabe, Y., Miyagawa-Tomita, S., Vincent, S. D., Kelly, R. G., Moon, A. M. and Buckingham, M. E. (2010) 'Role of mesodermal FGF8 and FGF10 overlaps in the development of the arterial pole of the heart and pharyngeal arch arteries', *Circ Res* 106(3): 495-503.
- Watkins, M. L., Rasmussen, S. A., Honein, M. A., Botto, L. D. and Moore, C. A. (2003) 'Maternal obesity and risk for birth defects', *Pediatrics* 111(5 Pt 2): 1152-8.
- Webster, W. S., Nilsson, M. and Ritchie, H. (2014) 'Therapeutic drugs that slow the heart rate of early rat embryos. Is there a risk for the human?', *Curr Pharm Des* 20(34): 5364-76.
- Wouters, B. G. and Koritzinsky, M. (2008) 'Hypoxia signalling through mTOR and the unfolded protein response in cancer', *Nat Rev Cancer* 8(11): 851-64.
- Xu, H., Morishima, M., Wylie, J. N., Schwartz, R. J., Bruneau, B. G., Lindsay, E. A. and Baldini, A. (2004) 'Tbx1 has a dual role in the morphogenesis of the cardiac outflow tract', *Development* 131(13): 3217-27.
- Zhang, J., Lin, Y., Zhang, Y., Lan, Y., Lin, C., Moon, A. M., Schwartz, R. J., Martin, J. F. and Wang, F. (2008) 'Frs2alpha-deficiency in cardiac progenitors disrupts a subset of FGF signals required for outflow tract morphogenesis', *Development* 135(21): 3611-22.
- Zhao, Z. (2012) 'Endoplasmic reticulum stress in maternal diabetes-induced cardiac malformations during critical cardiogenesis period', *Birth Defects Res B Dev Reprod Toxicol* 95(1): 1-6.
- Zheng, J. Y., Tian, H. T., Zhu, Z. M., Li, B., Han, L., Jiang, S. L., Chen, Y., Li, D. T., He, J. C., Zhao, Z. et al. (2013) 'Prevalence of symptomatic congenital heart disease in Tibetan school children', *Am J Cardiol* 112(9): 1468-70.

Figure 1. Effects of Low Oxygen Exposure of E9.5 Mouse Embryos on Outflow Tract Morphology; and Apoptosis, Differentiation and Proliferation of Second Heart Field Cells. (A-C) Comparison of three dimensional reconstructions of control (n=11) and exposed (8 hours, n=11) E10.5 outflow tracts (OFT) generated by optical projection tomography (OPT). Representative images of OFT from control (A) and exposed (B) embryos. The yellow lines indicate the measured distal OFT length, and the black lines indicate the angle measured between the distal and proximal OFT. (C) Graph showing the relationship between distal OFT length and angle between distal and proximal OFT at E10.5 for control (black dots) and exposed (red dots) embryos. The measurements for the images shown in panels A and B are indicated by open circles in black and red, respectively. Spearman correlation p values were 0.0086 (control) and 0.3221 (exposed). (D-L) Comparison of protein levels in control and exposed E9.5 mouse embryos using immunohistochemistry on sagittal paraffin sections. (D,E) active/pro Caspase 3 (n=10 control and 10 exposed, red), (G,H) myosin heavy chain (MHC, n=10 control and 19 exposed, green), (J,K) phospho-histone H3 (n=10 control and 10 exposed, green). Sections were counterstained with hemotoxylin (D,E, light blue) or TO-PRO-3 (G,H,J,K, red). For clarity, the brightness levels in the green channel only were increased. (F,I) Schematic diagrams indicating the relative positions of the second heart field (dark blue), pharyngeal endoderm (green), outflow tract (light blue) and left ventricle (red) and left atrium (orange) in a sagittal section of an E9.5 embryo. (L) Quantification of percentage phospho-histone H3-positive nuclei. Red dots indicate the quantification of the images shown in panels J and K respectively. In panels showing sections, rostral is to the top and caudal to the bottom. Location of the second heart field is indicated by brackets. SHF second heart field, OFT outflow tract, V ventricle, A atrium. Scale bars: 80 μ m (A,B), 130 μ m (D,E), 140 μ m (G,H), and 80 μ m (J,K). See also Figure S1.

Figure 2. Effects of Low Oxygen Exposure of E9.5 Mouse Embryos on FGF Signaling Targets in the Second Heart Field. (A-C) Comparison of gene expression levels of *Spry2* in control (A, n=11) and exposed (8 hours, B, n=12) E9.5 mouse embryos using whole-mount RNA *in situ* hybridization. (C) Quantification of levels of *Spry2* transcript in the second heart field (SHF). Red dots indicate the values for the embryos depicted in panels A and B. (D-F) Comparison of phospho-ERK1/2 (green) protein levels in control (D, n=12) and exposed (E, n=12) E9.5 mouse embryos using immunohistochemistry on sagittal paraffin sections. Nuclei were stained with TO-PRO-3 (red). (F) Quantification of phospho-ERK1/2 levels in the SHF. Red dots indicate the values for the embryos depicted in panels D and E. Location of the SHF is indicated by brackets. Scale bars: 500 μ m (A-B) and 80 μ m (D-E). See also Figure S2.

Figure 3. Effects of Low Oxygen Exposure of E9.5 Mouse Embryos on FGF Signaling Components in the Second Heart Field. (A-C) Comparison of gene expression levels of *Fgf8* in control (A, n=10) and exposed (8 hours, B, n=10) embryos using whole-mount RNA *in situ* hybridization. (C) Quantification of *Fgf8* transcript levels in the SHF. Red dots indicate the values for the embryos depicted in panels A and B. (D-K) Comparison of FGFR1 (green) protein levels in control (D, n=9) and exposed (8 hours, H, n=10) embryos using immunohistochemistry on sagittal paraffin sections. (E and I) Merged images showing FGFR1 (green), Golgi stained with GM130 (red) and nuclei stained with TO-PRO-3 (blue). (F and J) Magnified views of the boxed regions in panels E and I. (G) Quantification of the total FGFR1 protein expression levels in the SHF. (K) Quantification of the FGFR1 protein expression levels in the Golgi of the SHF. Red dots indicate the values for the embryos depicted in panels D and H. (L-N) Comparison of PDGFR β (red) protein levels in control (L, n=9) and exposed (8 hours, M, n=10) embryos using immunohistochemistry on sagittal paraffin sections. Nuclei were stained with TO-PRO-3 (blue). (N) Quantification of PDGFR β protein expression levels in the SHF. Red dots indicate the values for the embryos depicted in panels L and M. (O) Quantification from immunoblots of total protein levels of FGFR1 in whole E9.5 embryos exposed to normoxia (0 hours), or 5.5% oxygen for 1-4 hours. Location of the SHF is indicated by brackets. Scale bars: 500 μ m (A-B), 40 μ m (D-E, H-I, L-M) and 15 μ m (F,J). See also Figure S3.

Figure 4. SHF Cells in Embryos Exposed to Lowered Oxygen Levels *in utero* are Hypoxic and Induce the Unfolded Protein Response. (A-D) Comparison of cellular hypoxia levels in control

(A,B, n=8) and exposed (3 hours, C,D, n=8) E9.5 mouse embryos using immunohistochemistry against HypoxyprobeTM on sagittal paraffin sections (brown). Magnified views of the boxed regions in panels A and C are shown in B and D. (E-H) Comparison of HIF1 α (green) protein levels in control (E, n=12) and exposed (F, n=11) embryos using immunohistochemistry on sagittal paraffin sections. Nuclei were stained with TO-PRO-3 (red). (G-H) Quantification of the HIF1 α expression levels in the SHF (G) and myocardium (H). Red dots indicate the values for the embryos depicted in panels E and F. (I-K) Comparison of DDIT3 (green) protein levels in control (I, n=12) and exposed (8 hours, J, n=12) embryos using immunohistochemistry on sagittal paraffin sections. Nuclei were stained with TO-PRO-3 (red). (K) Quantification of the DDIT3 expression levels in the SHF. Red dots indicate the values for the embryos depicted in panels I and J. (L) Quantification of levels of spliced *Xbp1* transcripts in whole embryo RNA extracts from control (n=8) and exposed embryos. Exposure times in hours were 0.5 (n=6), 1 (n=5), 2 (n=7), 4 (n=7) and 8 (n=12). Location of the SHF is indicated by brackets. Scale bars: 80 μ m (A,C), 20 μ m (B,D), 80 μ m (E-F) and 140 μ m (I-J). See also Figure S4.

Figure 5. Hypoxia Induces the UPR and FGFR1 Loss *in vitro*. (A) Representative immunoblots (IB) of endogenous expression levels of FGFR1 (three bands representing fully glycosylated and partially glycosylated polypeptides), phospho-ERK1/2, total ERK1/2, phospho-eIF2 α and DDIT3 in mouse muscle satellite C2C12 cells exposed to 0.1% oxygen for the indicated times. β -tubulin was used as a loading control. Molecular marker sizes are shown in kDa. (B) Quantification of expression levels of FGFR1, phospho-ERK1/2 (relative to total ERK1/2), phospho-eIF2 α and DDIT3. See also Figure S5.

Figure 6. UPR-mediated Translation Inhibition Mediates FGFR1 Loss in Response to Hypoxic Exposure *in vitro* and *in vivo*. (A-D) Quantification of the expression levels of (A) FGFR1, (B) FLAG-XBP1 Δ DBD, (C) phospho-eIF2 α and (D) DDIT3 in C2C12 cells treated with 20 μ M 4 μ 8c. (E-H) Quantification of the expression levels of (E) FGFR1, (F) phospho-eIF2 α , (G) DDIT3, (H) phospho-ERK1/2 in C2C12 cells treated with 1 μ M GSK2606414. (I-K) PERK inhibitor predominantly rescued the immature forms of the FGFR1. (I) Immunoblot of endogenous FGFR1 in C2C12 cells exposed to hypoxia (0.1% oxygen) and treated with 1 μ M GSK2606414 (GSK). Three FGFR1 bands are detected representing fully glycosylated (140 kDa) and partially glycosylated (120 kDa and 95 kDa) polypeptides. For clarity, irrelevant lanes were removed (vertical lines) (J) Quantification of the absolute levels of mature (open circles) and immature forms (open squares) of FGFR1. (K) Quantification of the mature fully glycosylated FGFR1 polypeptide as a percentage of total FGFR1. (L-O) Comparison of FGFR1 (green) protein levels in unexposed and untreated control (L, n=17), unexposed and GSK2606414-treated (M, n=11), hypoxia exposed and untreated (N, n=16) and hypoxia exposed and GSK2606414-treated (O, n=17) embryos using immunohistochemistry on sagittal paraffin sections. FGFR1 (green), GM130 (Golgi, red) and TO-PRO-3 (nuclei, blue). (P-S) Comparison of phospho-ERK1/2 (green) protein levels in unexposed and untreated control (P, n=16), unexposed and GSK2606414-treated (Q, n=9), hypoxia exposed and untreated (R, n=16) and hypoxia exposed and GSK2606414-treated (S, n=15) embryos using immunohistochemistry on sagittal paraffin sections. phospho-ERK1/2 (green) and TO-PRO-3 (nuclei, red). (T) Quantification of the FGFR1 protein expression levels in the Golgi of the SHF. (U) Quantification of the total FGFR1 protein expression levels in the SHF. (V) Quantification of phospho-ERK1/2 levels in the SHF. Red dots indicate the values for the embryos depicted in panels K-R. Location of the SHF is indicated by brackets. Scale bar: 40 μ m (L-O), 80 μ m (P-S).

756 **Table 1. *In utero* Low Oxygen Exposure Induces Heart Defects**

757

	Heart morphology					
Exposure stage	Normal	Abnormal	% Abnormal	p value*	% Resorbed	p value*
Control	31	2	6.1		8.3	
E7.5	27	0	0	0.30	3.8	0.32
E8.5	33	7	17.5	0.13	8.9	0.62
E9.5	27	21	43.8	0.0001	11.9	0.42
E10.5	29	7	19.4	0.10	33.9	0.004

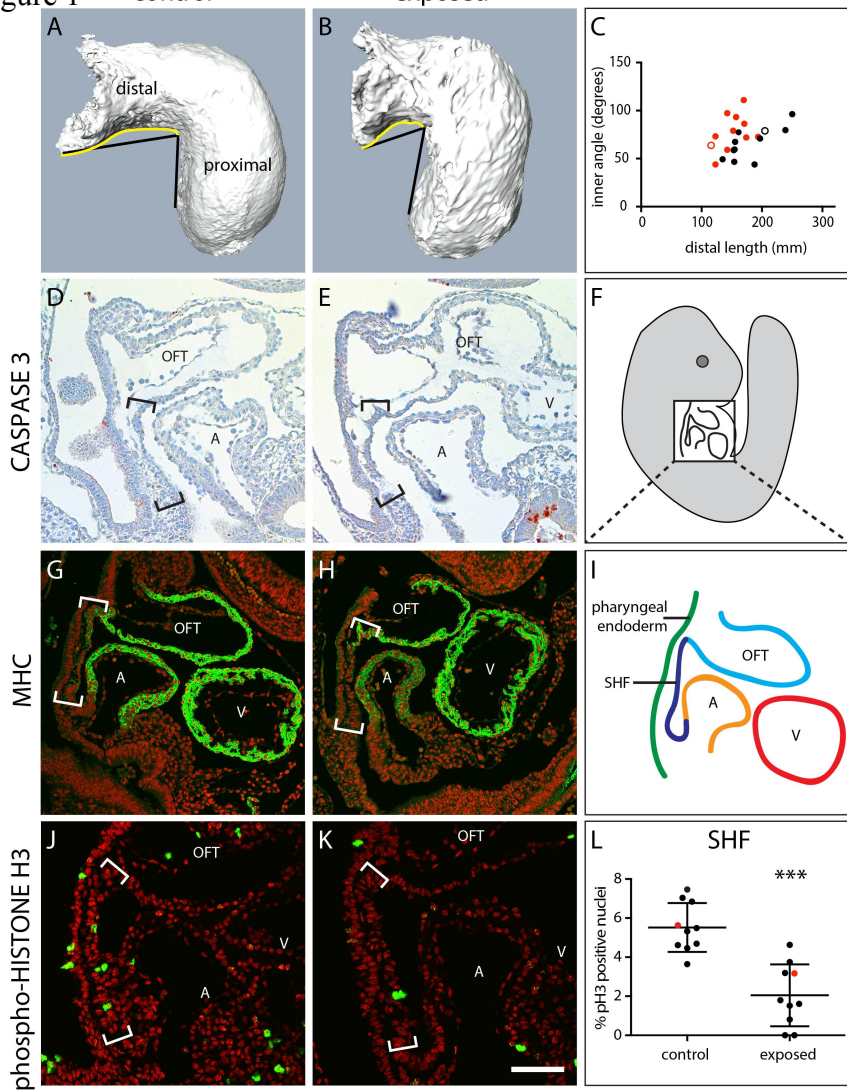
758 * one-tailed Fisher's exact test.

759

760

761

Figure 1 control exposed



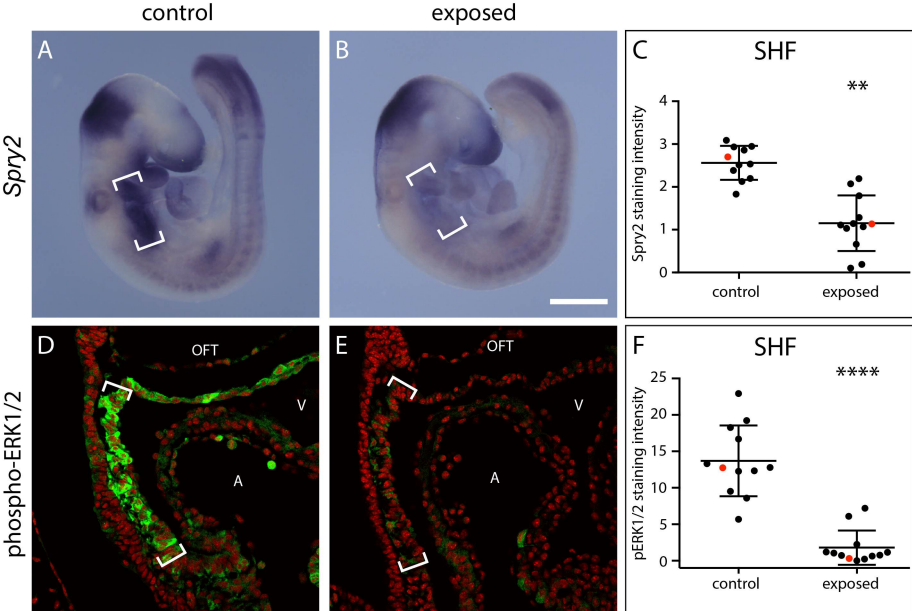
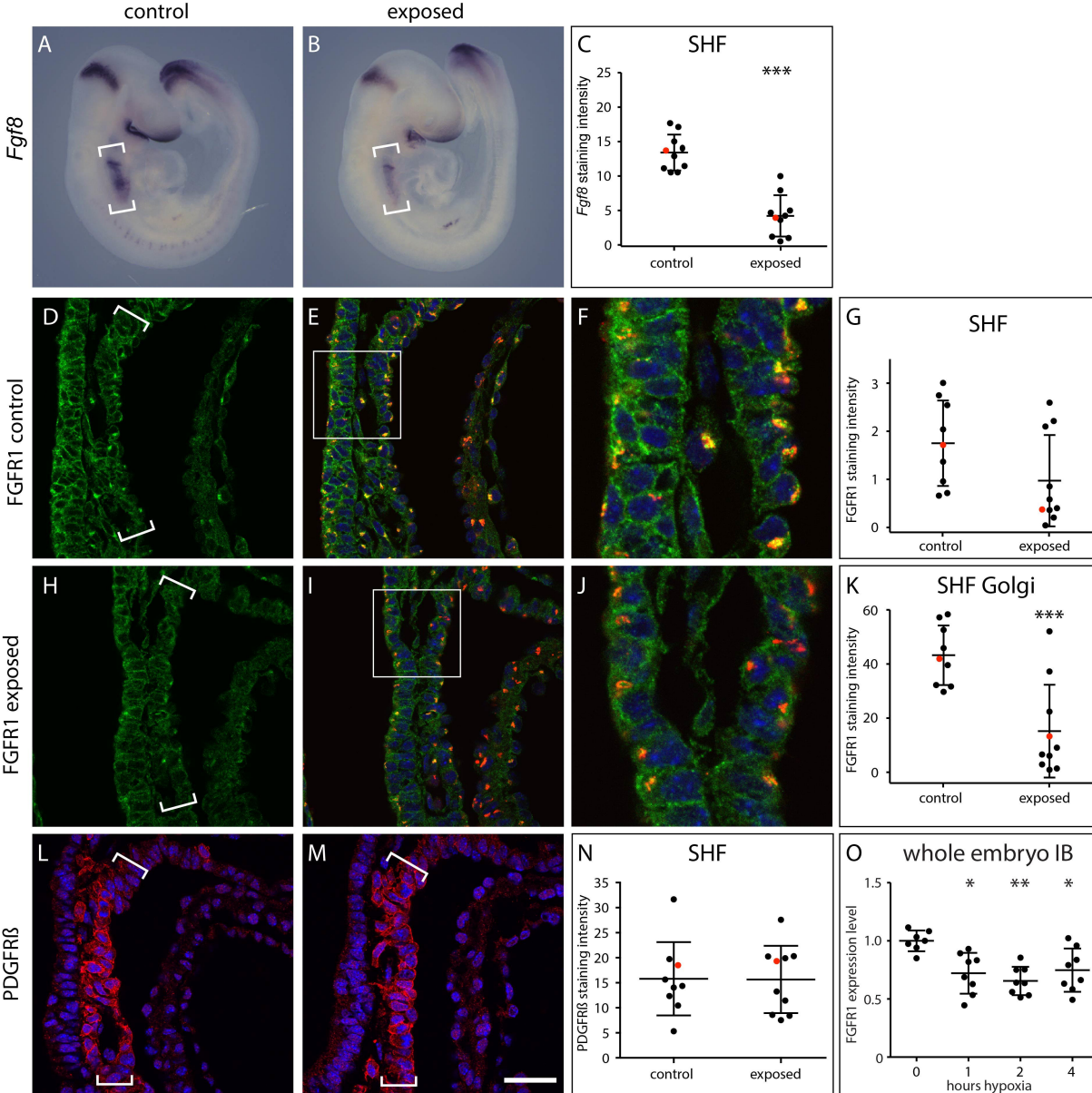


Figure 2

Figure 3



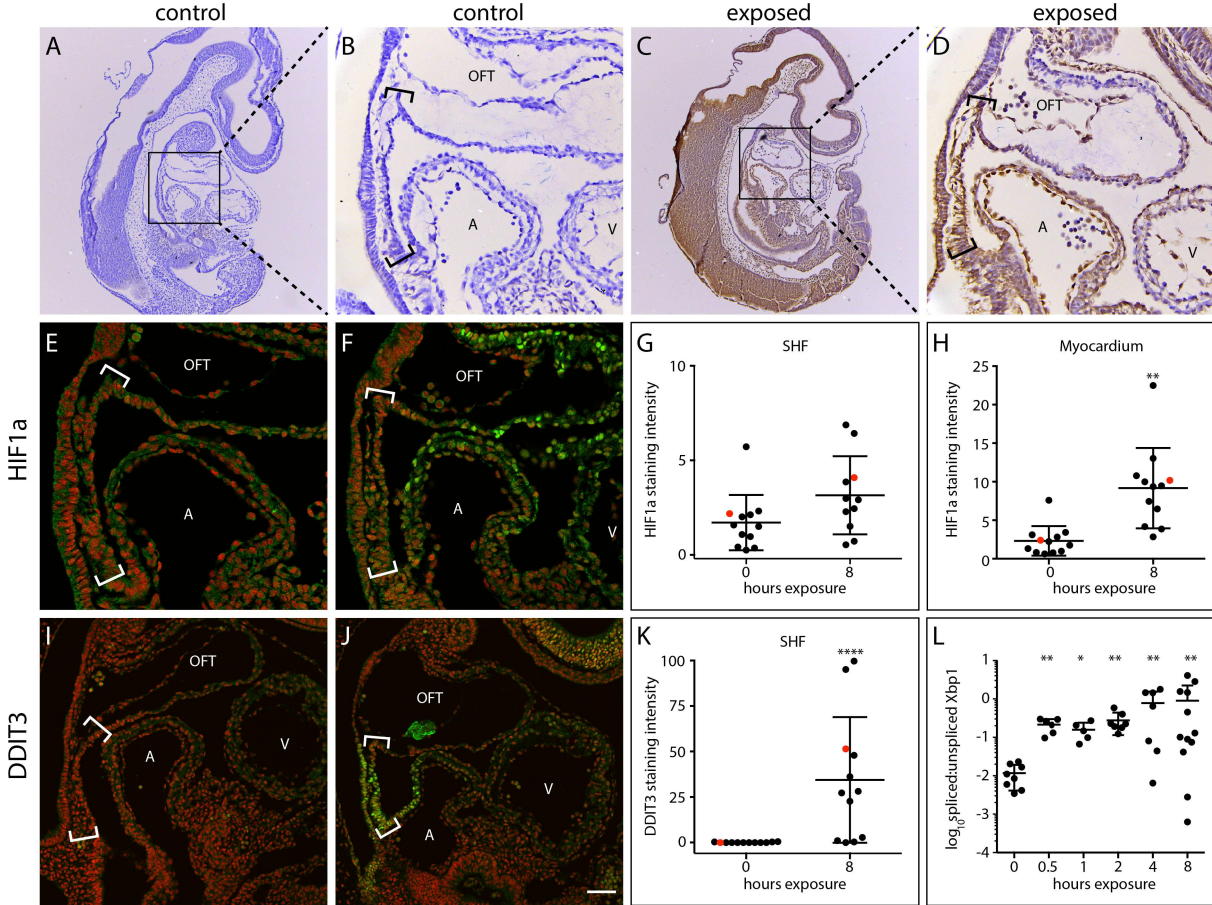
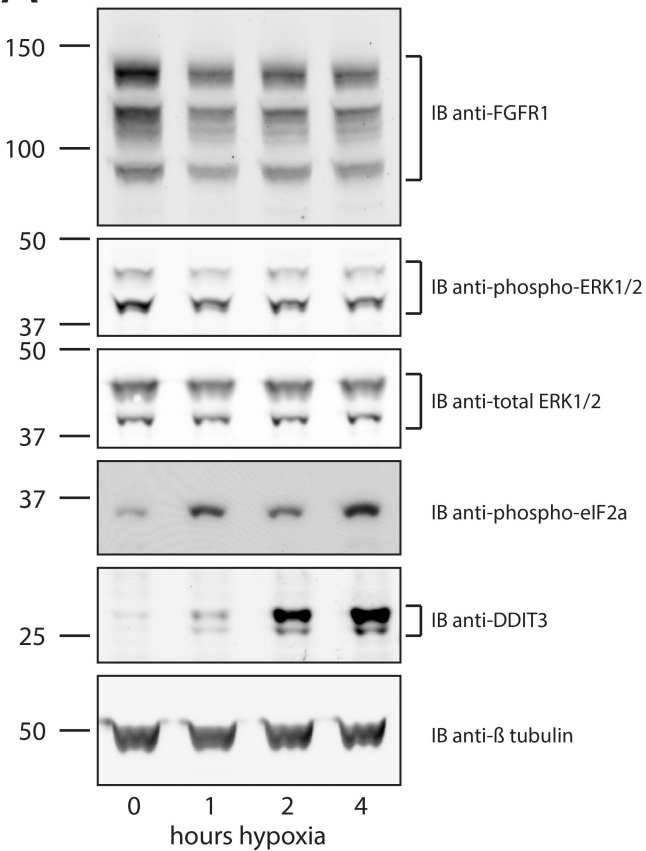
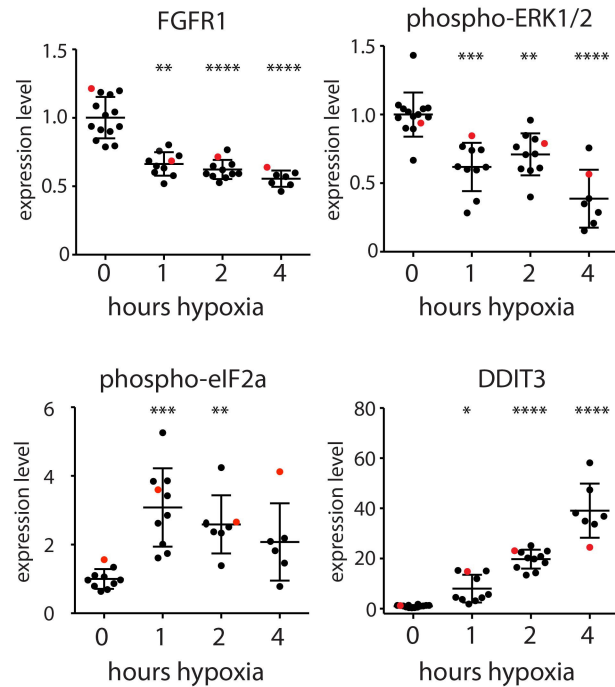


Figure 4

A**B****Figure 5**

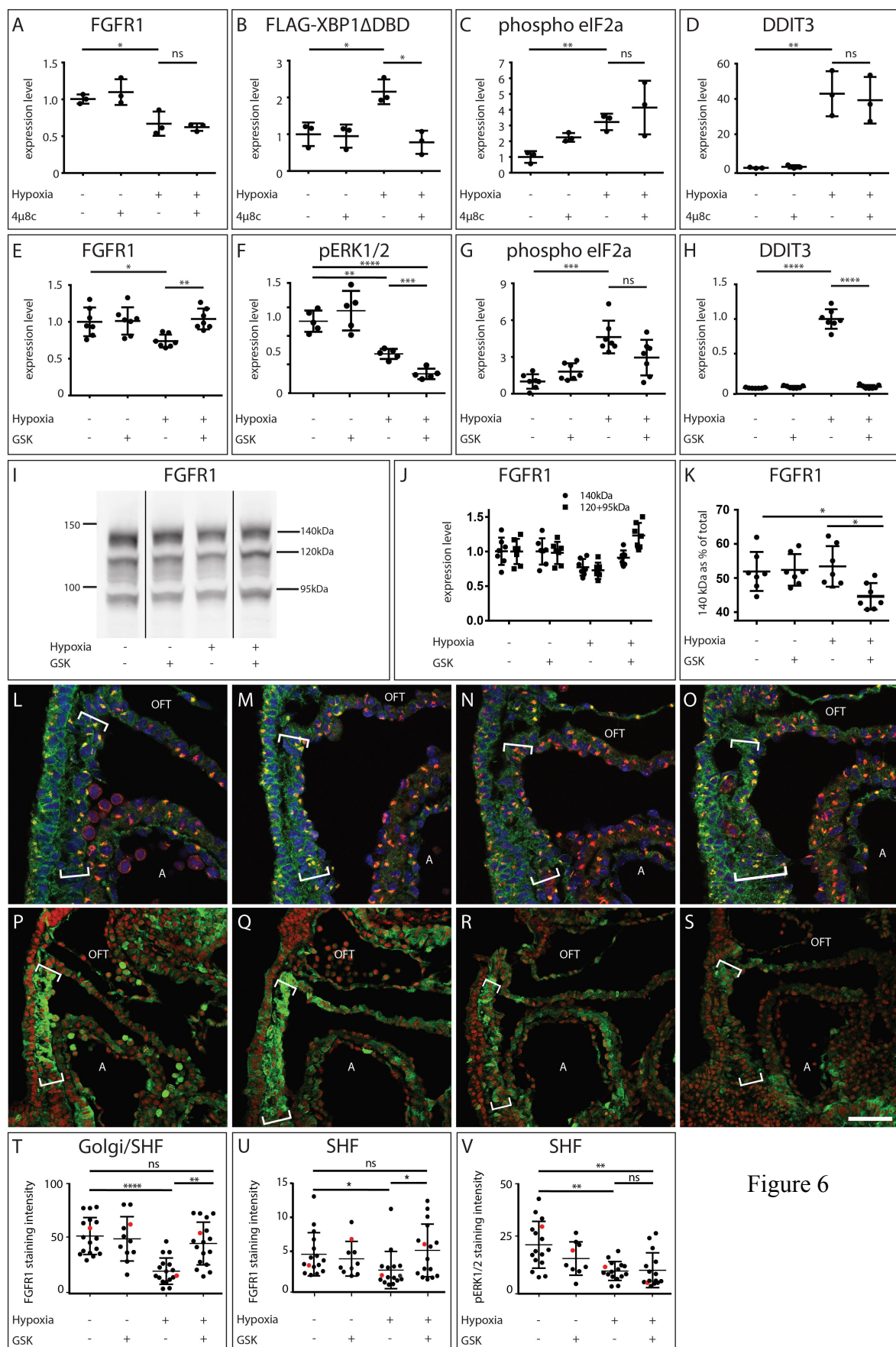


Figure 6

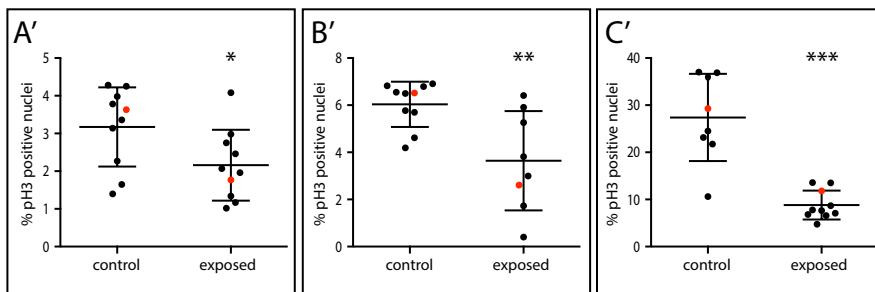
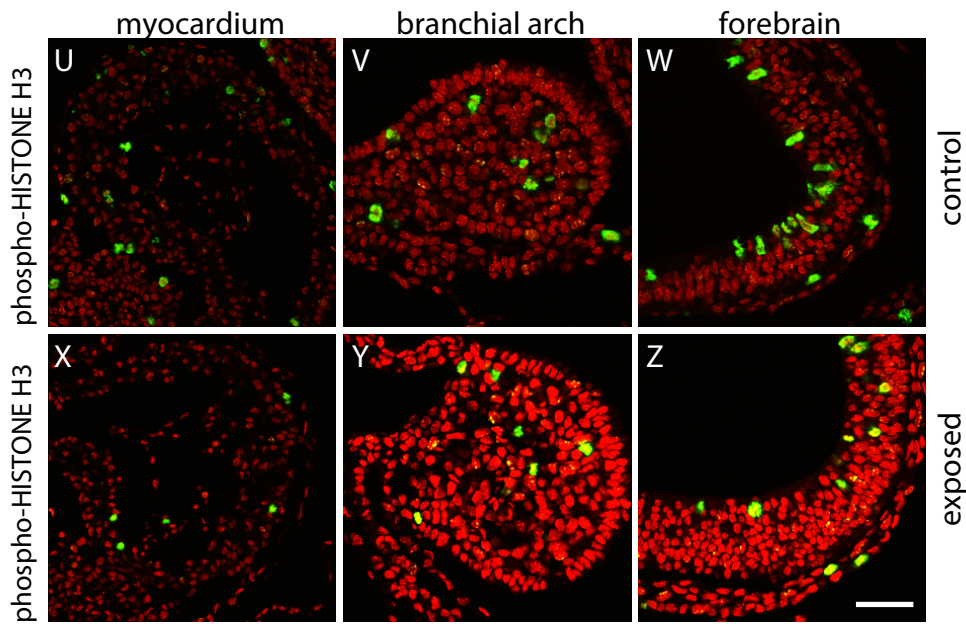
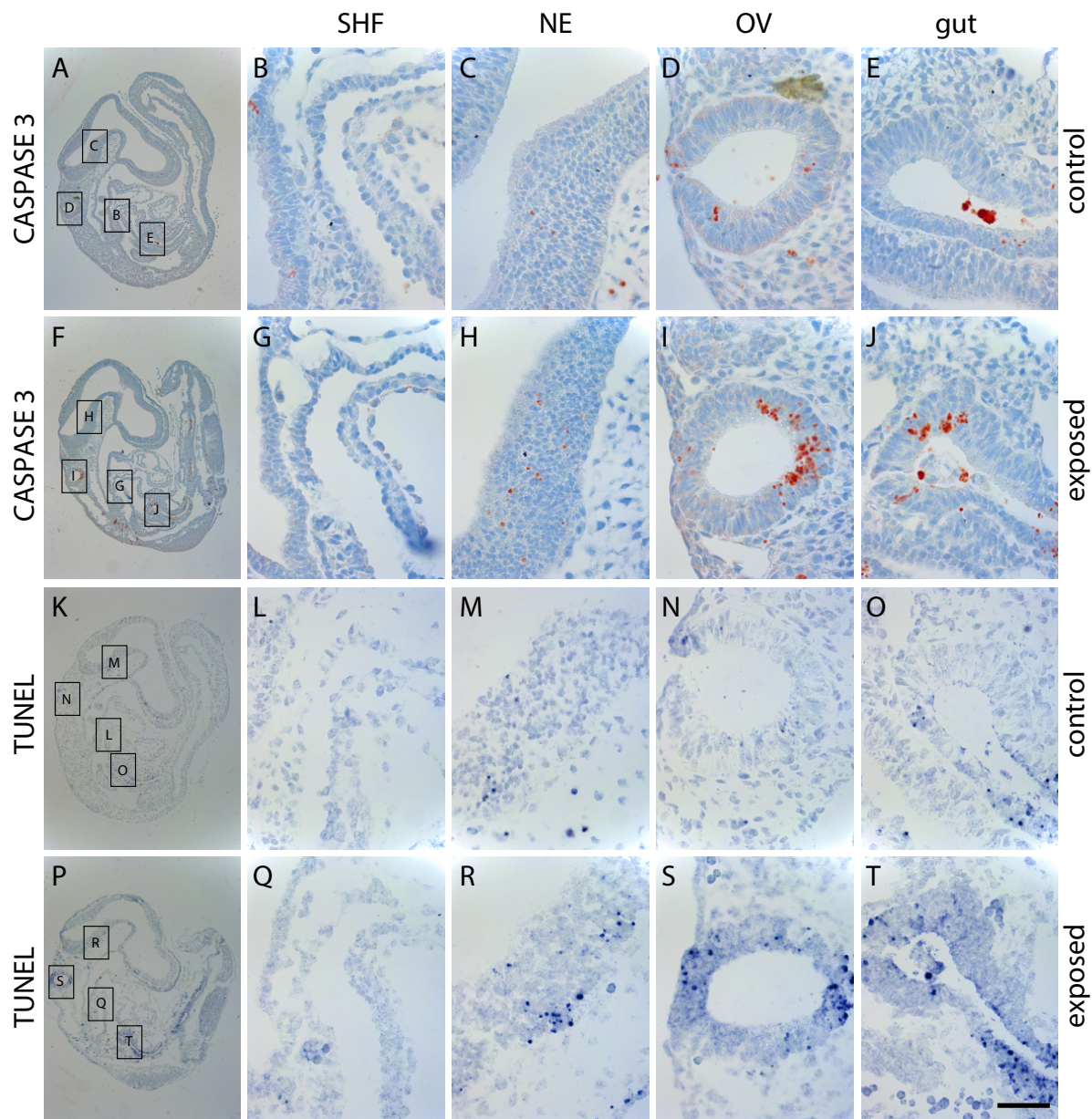


Figure S1

Figure S1. Effects of Low Oxygen Exposure of E9.5 Mouse Embryos on Apoptosis and Proliferation of Second Heart Field Cells. Related to Figure 1.

(A-J) Comparison of active/pro Caspase 3 protein levels (red) in control (A-E, n=10) and exposed (8 hours, F-J, n=10) E9.5 mouse embryos using immunohistochemistry on sagittal paraffin sections. (A and F) Low magnification images of representative sections. (B-E and G-J) High magnification images of the boxed regions of panels A and F showing the second heart field (SHF), neuroectoderm (NE), otic vesicle (OV) and gut. Sections were counterstained with haematoxylin (light blue). (K-T) Comparison of TUNEL staining (dark blue) on adjacent sagittal paraffin sections of control (K-O, n=10) and exposed (P-T, n=10) E9.5 mouse embryos. (K and P) Low magnification images of representative sections. (L-O and Q-T) High magnification images of the boxed regions of panels K and P showing the second heart field (SHF), neuroectoderm (NE), otic vesicle (OV) and gut. (U-C') Comparison of phospho- histone H3 protein levels (green) in control (U-W, n=10) and exposed (X-Z, n=10) E9.5 mouse embryos using immunohistochemistry on sagittal paraffin sections. Nuclei were stained with TO- PRO-3 (red). Representative sections of myocardium (U,X), branchial arch (V,Y) and forebrain (W,Z) are shown. (A'-C') Quantification of percentage of phospho- histone H3 positive nuclei for each tissue. Red dots indicate the quantification of the images shown in panels (U-Z). Scale bars: 560 μ m (A, F, K and P), 70 μ m (B-E, G-J, L-O and Q-T), 110 μ m (U,X) and 50 μ m (V,W,Y,Z). Graph shows mean and standard deviation. * $p < 0.05$, ** $p < 0.01$, *** $p < 0.001$

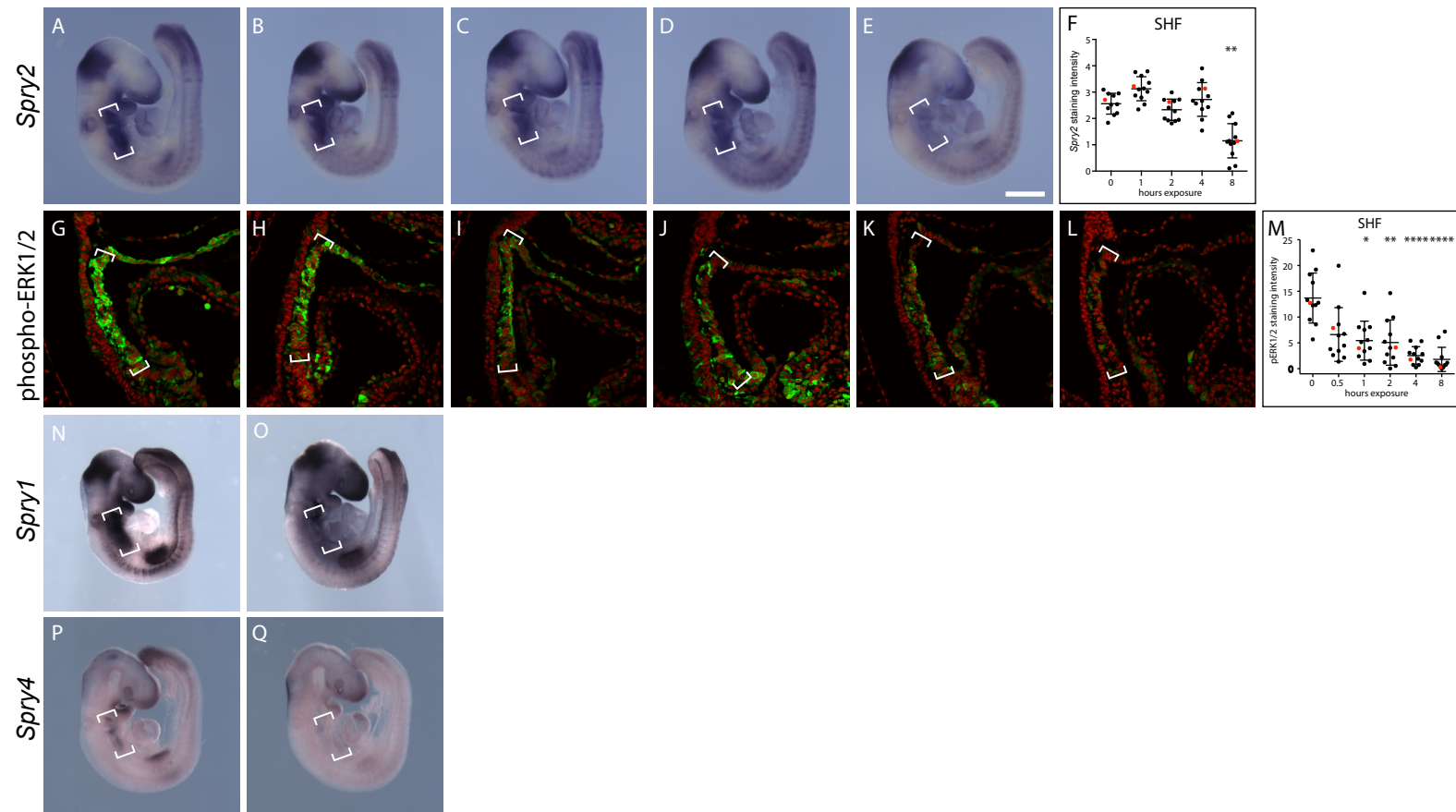
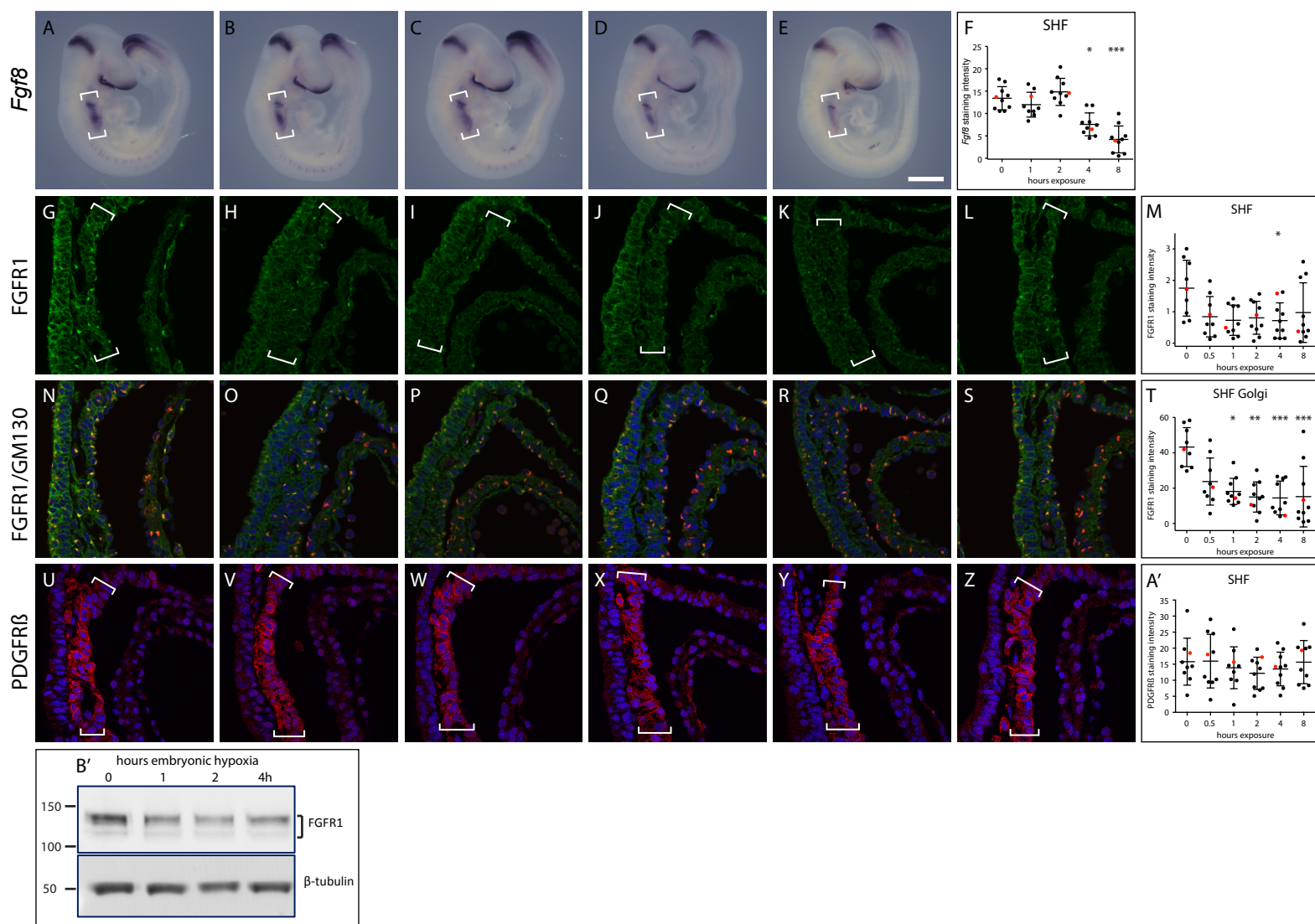


Figure S2. Effects of Low Oxygen Exposure of E9.5 Mouse Embryos on FGF Signaling Targets in the Second Heart Field. Related to Figure 2.

(A-F) Comparison of gene expression levels of *Spry2* in control (A, n=11) and exposed (B-E) E9.5 mouse embryos using whole-mount RNA in situ hybridization. Exposure times in hours were 1 (B, n=12), 2 (C, n=12), 4 (D, n=12) and 8 (E, n=12). (F) Quantification of levels of *Spry2* transcript in the second heart field (SHF). Red dots indicate the values for the embryos depicted in panels A-E. (G-M) Comparison of phospho-ERK1/2 (green) protein levels in control (G, n=12) and low oxygen exposed (H-L) E9.5 mouse embryos using immunohistochemistry on sagittal paraffin sections. Exposure times in hours were 0.5 (H, n=12), 1 (I, n=12), 2 (J, n=12), 4 (K, n=12) and 8 (L, n=12). Nuclei were stained with TO-PRO-3 (red). (M) Quantification of levels of phospho-ERK1/2 in the SHF. Red dots indicate the values for the embryos depicted in panels G-L. (N-O) Comparison of gene expression levels of *Spry1* in control (N, n=5) and 8 hour exposed (O, n=5) E9.5 mouse embryos using whole-mount RNA in situ hybridization. (P-Q) Comparison of gene expression levels of *Spry4* in control (P, n=12) and 8 hour exposed (Q, n=14) E9.5 mouse embryos using whole-mount RNA in situ hybridization. In panels showing sections, rostral is to the top and caudal to the bottom. Location of the SHF is indicated by brackets. OFT = outflow tract, v = ventricle, a = atrium. Scale bars: 500 μ m (A-E, N-Q) and 40 μ m (G-L). Graph shows mean and standard deviation. * $p < 0.05$, ** $p < 0.01$, **** $p < 0.0001$.



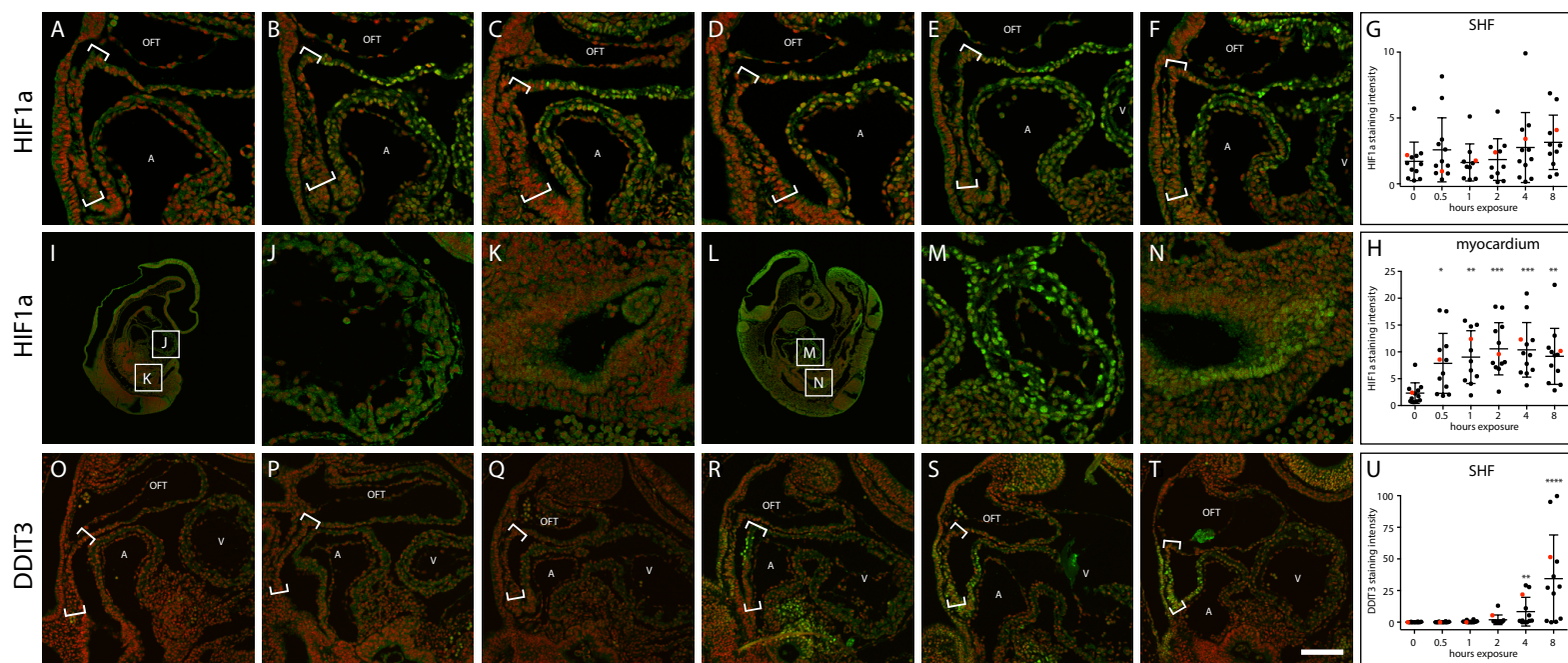


Figure S4. Cells in Embryos Exposed to Lowered Oxygen Levels in utero are Hypoxic and Induce the Unfolded Protein Response. Related to Figure 4.

(A-H) Comparison of HIF1α (green) protein levels in control (A, n=12) and exposed (B-F) E9.5 mouse embryos using immunohistochemistry on sagittal paraffin sections. Exposure times in hours were 0.5 (B, n=12), 1 (C, n=10), 2 (D, n=11), 4 (E, n=12) and 8 (F, n=11). Nuclei were stained with TO-PRO-3 (red). (G-H) Quantification of levels of HIF1α in the SHF (G) and myocardium (H). Red dots indicate the values for the embryos depicted in panels A-F. (I-N) Comparison of HIF1α (green) protein levels in control (I) and low oxygen exposed (L) E9.5 mouse embryos. Magnified views of the boxed areas in panels I and L showing HIF1α staining in myocardium (J and M) and gut (K and N). (O-U) Comparison of DDIT3 (green) protein levels in control (O, n=12) and low oxygen exposed (P-T) E9.5 mouse embryos using immunohistochemistry on sagittal paraffin sections. Exposure times in hours were 0.5 (P, n=12), 1 (Q, n=12), 2 (R, n=12), 4 (S, n=12) and 8 (T, n=12). Nuclei were stained with TO-PRO-3 (red). (U) Quantification of levels of DDIT3 in the SHF. Red dots indicate the values for the embryos depicted in panels O-T. In panels showing sections, rostral is to the top and caudal to the bottom. Scale bars: 80 μm (A-F), 570 μm (I and L), 70 μm (J-K, M- N) and 140 μm (O-T). Location of the SHF is indicated by brackets. OFT = outflow tract, v = ventricle, a = atrium. Graph shows mean and standard deviation. * p<0.05, ** p<0.01, *** p<0.001, **** p<0.0001.

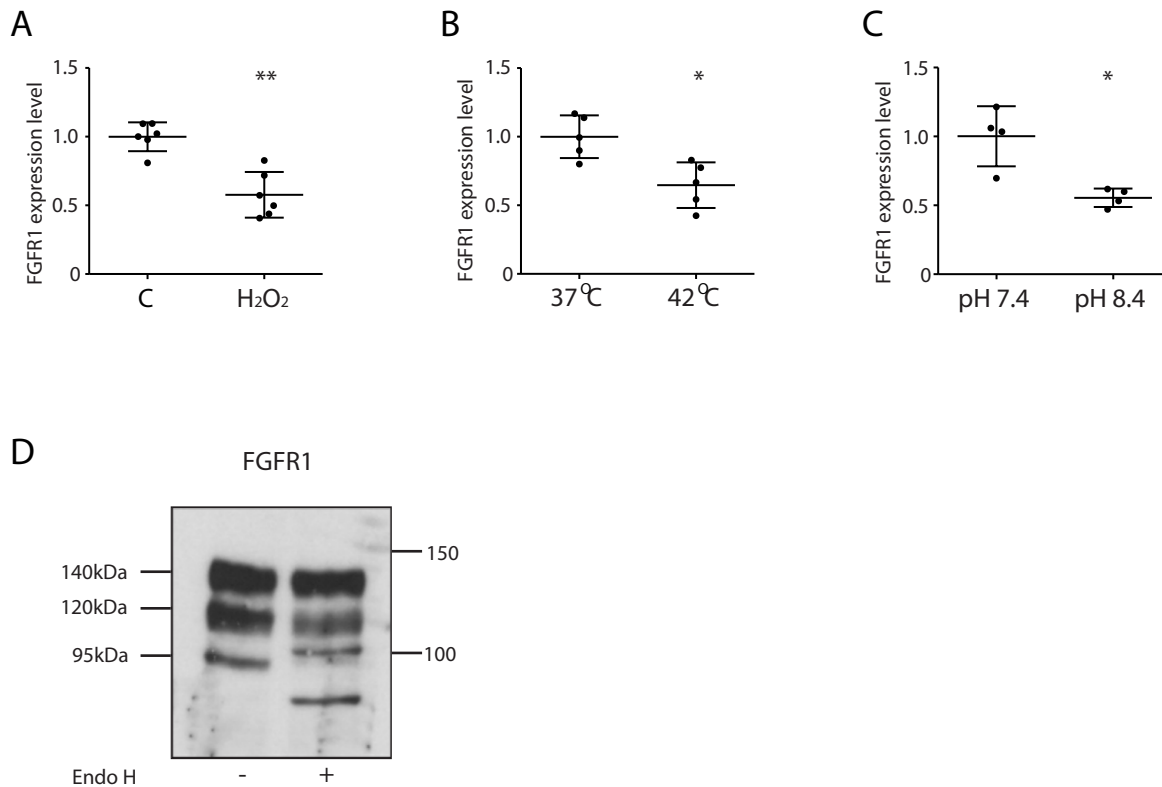


Figure S5. Quantification of FGFR1 Protein Levels in Embryos and Cells by Immunoblot. Related to Figure 5.

(A-C) Quantification graphs for FGFR1 in cells exposed for 2 hours to (A) 0.1 mM hydrogen peroxide, (B) heat shock at 42°C, or (C) alkaline pH (culture under 0.1% CO₂ atmosphere). (D) Immunoblot of endogenous FGFR1 in mouse muscle satellite C2C12 cells. Three bands are detected (140 kDa, 120 kDa and 95 kDa; left lane). Endoglycosidase H (Endo H; right lane) does not cleave the fully glycosylated 140 kDa polypeptide, but does cleave the partially glycosylated (120 kDa, 95 kDa) polypeptides. Molecular marker sizes are shown in kDa. Graph shows mean and standard deviation. * $p < 0.05$, ** $p < 0.01$.

SUPPLEMENTARY TABLE

Table S1. Short term Gestational Hypoxia Induces Heart Defects

				Type of heart defect observed								
Exposure stage	Embryos examined	Normal	Abnormal	VSD	muscular VSD	OA	DORV	TGA	ASD	PTA	SOTV	TVA
control	33	31	2	2	1	0	0	0	0	0	0	0
E7.5	27	27	0	0	0	0	0	0	0	0	0	0
E8.5	40	33	7	6	1	3	2	1	1	0	2	0
E9.5	48	27	21	18	1	7	10	3	3	1	1	1
E10.5	36	29	7	5	2	2	0	0	2	0	3	0

Note that a particular embryo may have more than one type of defect.

Pregnant mice were exposed to 5.5% oxygen for 8 hours on the indicated day of gestation. Mice were returned to normoxia, and embryos allowed to develop until E17.5, when heart morphology was analyzed. VSD: membranous ventricular septal defect; muscular VSD: muscular ventricular septal defect; OA: overriding aorta; DORV: double-outlet right ventricle; TGA: transposition of the great arteries; ASD: atrial septal defect; PTA: persistent truncus arteriosus; SOTV: straddling overriding tricuspid valve; TVA: tricuspid valve atresia

SUPPLEMENTAL MATERIALS AND METHODS

Optical projection tomography

For analysis of E10.5 OFTs, embryo torsos immunostained with MF 20 were dehydrated in methanol and cleared for at least 24 hours in 1:2 benzoic acid/benzyl benzoate (BABB). These were superglued directly to the mounting post of the OPT scanner. For whole E17.5 hearts, hearts were dissected from Bouin's fixed embryos stored in 70% ethanol, rehydrated to water, then dehydrated in methanol and cleared in BABB for at least 24 hours. Single hearts were placed in a cut-off and sealed glass Pasteur pipette, and attached to the mounting post. OPT scanning was performed using a custom microscope controlled by purpose-built software OPTimum (James Springfield, Institute for Molecular Biosciences, University of Queensland, Australia). 800-1,200 images in the FITC channel were collected per sample. These were reconstructed using nRecon (Bruker microCT, Belgium). Data were rendered in Amira 5.5.0 (FEI Visualization Services Group, USA). E17.5 heart morphology was analyzed directly in Amira. To quantitate OFT dimensions, reconstructions of OFTs were first rotated to the same orientation using Amira. 2D views were then exported in PNG format, and the OFT angle and length measured using ImageJ 1.49 (NIH, USA).

Immunohistochemistry

For immunohistochemistry, embryos were harvested at E9.5, fixed overnight in 4% paraformaldehyde at 4°C, paraffin embedded and sectioned in the sagittal plane. To minimize inter-slide staining variation, tissue arrays were made by putting single sections from 12-20 different embryos on a single slide, and slides were processed using a Shandon Sequenza® Immunostaining Center (Thermo Scientific). Antigen retrieval for all antibodies except active/pro Caspase 3 was done using TE buffer (Moreau et al., 2014). For active/pro Caspase 3, slides were boiled in 10 mM Sodium Citrate, 0.05% Tween 20, pH 6.0 for 25 minutes. Slides were mounted in Mowiol® with DABCO (Allan, 1999). Images were captured on either a LSM 7 Duo or a LSM 710 upright confocal microscope (Carl Zeiss). For detecting FGFR1 or HIF1 α in paraffin sections, biotinylated donkey anti-rabbit secondary and streptavidin Cy3 tertiary reagents were used. For detecting active/pro Caspase 3 and Hypoxyprobe™ in paraffin sections, ImmPRESS™ secondary reagent and 3-amino-9-ethylcarbazole (AEC for Caspase 3; Sigma Aldrich) or 3, 3'-diaminobenzidine (DAB for Hypoxyprobe™; Sigma Aldrich) was used.

Antibodies Used for immunodetection

Target	Name	Catalog number	Species and type	Supplier	Dilution for IHC	Dilution for IB
Primary antibodies						
active/pro Caspase 3		ab13847	rabbit polyclonal	Abcam	1:200	na
Myosin II heavy chain	MF 20		mouse monoclonal	Developmental Studies Hybridoma Bank	1:100	na
phospho-histone H3	(Ser 10)-R	sc-8656	rabbit polyclonal	Santa Cruz Biotechnology	1:200	na
phospho-p44/42 MAPK (Erk1/2) (Thr202/Tyr204)	D13.14.4 E	4370	rabbit monoclonal	Cell Signaling Technology	1:200	1:1,000
p44/42 MAPK (Erk1/2)		9102	rabbit polyclonal	Cell Signaling Technology	na	1:1,000
FGFR1	D8E4	9740	rabbit monoclonal	Cell Signaling Technology	1:400	1:1,500
GM130		610822	mouse monoclonal	BD Transduction Laboratories	1:400	na
PDGFR β	958	sc-432	rabbit polyclonal	Santa Cruz Biotechnology	1:50	na
Hypoxyp TM FITC	4.3.11.3		Mouse monoclonal	Hypoxyp TM , Inc.	1:400	na
HIF1 α		NB100-449	rabbit polyclonal	Novus Biologicals	1:400	na
DDIT3	F-168	sc-575	rabbit polyclonal	Santa Cruz Biotechnology	1:50	1:500
phospho eIF2 α (Ser51)	D9G8	3398	rabbit monoclonal	Cell Signaling Technology	na	1:1,000
β -tubulin	E7		mouse monoclonal	Developmental Studies Hybridoma Bank	na	1:500
FLAG [®]	M2	F1804	mouse monoclonal	Sigma-Aldrich	na	1:1,000
Secondary Antibodies						
Donkey anti-		711-165-		Jackson	1:500	na

rabbit Cy TM 3		152		ImmunoResearch		
Donkey anti-goat AlexaFluor® 488		A-11055		Life Technologies	1:500	na
Donkey anti-mouse AlexaFluor® 488		715-545-151		Jackson ImmunoResearch	1:500	na
Goat anti-mouse IRDye® 800CW		926-32210		LI-COR	na	1:10,000
Goat anti-rabbit AlexaFluor® 680		A-21109		Life Technologies	na	1:5,000
Donkey anti-rabbit biotinylated		711-065-152		Jackson ImmunoResearch	1:500	na
ImmPRESS TM (Peroxidase) Polymer anti-mouse Ig Reagent		MP-7402		Vector Laboratories	1:1	na
ImmPRESS TM (Peroxidase) Polymer anti-rabbit Ig Reagent		MP-7401		Vector Laboratories	1:1	na
Tertiary reagents						
Streptavidin Cy TM 3		GTX85902		GeneTex	1:1,000	na
Nuclear stain						
TO-PRO®-3 Iodide		T3605		Life Technologies	1:10,000	na

RNA *in situ* hybridization probes

cDNA probes used were as follows: *Spry1* (Addgene plasmid # 22091, Minowada et al., 1999), *Spry2* (Addgene plasmid # 22097, Minowada et al., 1999), *Spry4* (Addgene plasmid # 22093, (Minowada et al., 1999), and *Fgf8* (Mahmood et al., 1995).

Cell culture and immunoblots

Mouse muscle satellite C2C12 cells (ATCC) were cultured in IMDM medium with glutamine (Life Technologies) and 10% fetal bovine serum (Life Technologies) on 40 mm Steriplan®

glass petri dishes (DURAN) in 5% CO₂. C2C12 cells were verified as free from mycoplasma contamination using the MycoAlert Detection Kit (Lonza). Hypoxic exposure of cells was done using a H35 Hypoxystation (Don Whitley Scientific). Culture medium was equilibrated in 0.1% O₂ overnight prior to use. Culture dishes were transferred to the workstation, rinsed once with hypoxia-equilibrated medium, and incubated in fresh hypoxia-equilibrated medium for the indicated times. For the study of UPR inhibitors, cells were incubated for 2 hours in the normoxic or hypoxia-equilibrated medium containing 20 μ M IRE1 inhibitor 4 μ 8c (Sigma Aldrich) or 1 μ M PERK inhibitor GSK2606414 (Selleck Chemicals) or equivalent volume of DMSO as a control. Whole cell protein extracts and immunoblots were performed by standard methods, with detection using either HRP-labeled secondary antibodies and SuperSignal West Pico chemiluminescent substrate (Thermo Fisher) or fluorescently-labeled secondary antibodies and the Li-Cor Odyssey Infrared Imaging System.

Quantification methods

Staining intensity of immunohistochemistry on paraffin sections was quantified using ImageJ 1.49 (NIH, USA). Briefly, LSM files generated by confocal microscopy were imported into ImageJ. The region of interest (ROI) was manually defined, and the image was thresholded to remove background. Identical thresholding values were used for all images of each experiment. The signal above threshold was quantified, and normalized to ROI area. For quantitation of FGFR1 proteins levels in the Golgi, stacks of confocal LSM images from sections co-stained with FGFR1 and GM130 were imported into ImageJ. The ROI was manually defined in the GM130 channel, and all signal outside this area was removed. The GM130 channel was thresholded to remove background, using identical values for all images, and the intensity of GM130 staining quantified. The area of GM130 staining in the ROI was used to make a selection mask, which was then applied to the FGFR1 channel. The FGFR1 channel was thresholded to remove background using identical values for all images, and the intensity of FGFR1 staining in the GM130-expressing domain of the ROI was quantified. For proliferation measurement, the percentage of phospho-histone H3 positive cells in each embryo was calculated as the ratio of combined total number of phospho-histone H3 positive cells against the combined total number To-Pro3+ nuclei from three independent sections from the same embryo. Staining intensity of RNA wholemount *in situ* hybridization images was also quantified using ImageJ. Stained embryos were photographed using a M125 dissection microscope with DFC450 camera (Leica microsystems GmbH, Germany), using

identical lighting and camera settings for all embryos stained for the same transcript. TIFF files were imported into ImageJ and changed to 8-bit grayscale. The ROI was manually defined, thresholded to remove background with identical settings for all images, and the integrated density in the ROI measured. Immunoblots analyzed by chemiluminescence were digitized using a FLA-5100 scanner (Fujifilm, Japan), and converted to TIFF format using ImageJ. Immunoblots analyzed by Odyssey Imager (LI-COR) were scanned at high resolution and saved as TIFF files. In both cases, bands were quantitated using Gelanalyzer (gelanalyzer.com).

Analysis of embryonic apoptosis

Two adjacent sagittal sections of each embryo (n=10 control and n=10 exposed) were stained for active/pro Caspase 3 and the other for TUNEL. These were taken from roughly the same sagittal plane from every embryo to ensure a similar area was surveyed across all embryos. One view field per section was counted for each of the SHF, OFT, ventricular myocardium, posterior part of the neural tube, otic vesicle and gut.

Image manipulation

For clarity, in Figure 1 panels J and K the brightness levels in the green channel only (phospho-histone H3) were increased.

SUPPLEMENTARY REFERENCES

Mahmood, R., Bresnick, J., Hornbruch, A., Mahony, C., Morton, N., Colquhoun, K., Martin, P., Lumsden, A., Dickson, C., and Mason, I. (1995). A Role for Fgf-8 in the Initiation and Maintenance of Vertebrate Limb Bud Outgrowth. *Curr Biol* 5, 797-806.

Minowada, G., Jarvis, L.A., Chi, C.L., Neubuser, A., Sun, X., Hacohen, N., Krasnow, M.A., and Martin, G.R. (1999). Vertebrate Sprouty Genes Are Induced by Fgf Signaling and Can Cause Chondrodysplasia When Overexpressed. *Development* 126, 4465-4475.

Allan, V.J. (1999) *Protein Localization by Fluorescence Microscopy*, Oxford, United Kingdom: Oxford University Press.

Moreau, J. L., Artap, S. T., Shi, H., Chapman, G., Leone, G., Sparrow, D. B. and Dunwoodie, S. L. (2014) 'Cited2 is required in trophoblasts for correct placental capillary patterning', *Dev Biol* 392(1): 62-79.